Thin and thinner: Sea ice mass balance measurements during SHEBA

Donald K. Perovich,[1] Thomas C. Grenfell,[2] Jacqueline A. Richter-Menge,[1] Bonnie Light,[2] Walter B. Tucker III,[1] and Hajo Eicken[3]

Received 3 August 2001; revised 25 February 2002; accepted 29 April 2002; published 20 March 2003.

[1] As part of a large interdisciplinary study of the Surface Heat Budget of the Arctic Ocean (SHEBA), we installed more than 135 ice thickness gauges to determine the sea ice mass balance. While installing these gauges during the fall of 1997, we found that much of the multiyear ice cover was only 1 m thick, considerably thinner than expected. Over the course of the yearlong field experiment we monitored the mass balance for a wide variety of ice types, including first-year ice, ponded ice, unponded ice, multiyear ice, hummocks, new ridges, and old ridges. Initial ice thicknesses for these sites ranged from 0.3 to 8 m, and snow depths varied from a few centimeters to more than a meter. However, for all of their differences and variety, these thickness gauges sites shared a common trait: at every site, there was a net thinning of the ice during the SHEBA year. The thin ice found in October 1997 was even thinner in October 1998. The annual cycle of ice thickness was also similar at all sites. There was a steady increase in thickness through the winter that gradually tapered off in the spring. This was followed by a steep drop off in thickness during summer melt and another tapering in late summer and early fall as freeze-up began. Maximum surface melting was in July, while bottom ablation peaked in August. Combining results from the sites, we found an average winter growth of 0.51 m and a summer melt of 1.26 m, which consisted of 0.64 m of surface melt and 0.62 m of bottom melt. There was a weak trend for thicker ice to have less winter growth and greater net loss for the year; however, ice growth was also impacted by the snow depth. Considerable variability was observed between sites in both accretion and ablation. The total accretion during the 9-month growth season ranged from zero for thick ridged ice to more than a meter for young ice. Ponds tended to have a large amount of surface melting, while ridges had considerable bottom ablation. *INDEX TERMS:* 4540 Oceanography: Physical: Ice mechanics and air/sea/ice exchange processes; 4207 Oceanography: General: Arctic and Antarctic oceanography; 3349 Meteorology and Atmospheric Dynamics: Polar meteorology; *KEYWORDS:* Arctic, sea ice, mass balance, sea ice melting, melt ponds

Citation: Perovich, D. K., T. C. Grenfell, J. A. Richter-Menge, B. Light, W. B. Tucker III, and H. Eicken, Thin and thinner: Sea ice mass balance measurements during SHEBA, *J. Geophys. Res.*, *108*(C3), 8050, doi:10.1029/2001JC001079, 2003.

1. Introduction

[2] Large-scale general circulation models indicate that Arctic sea ice may be a sensitive indicator of climate change and that the details of the complex atmosphere-ice-ocean interaction are not well understood [*Spelman and Manabe*, 1984; *Washington and Meehl*, 1986; *Dickinson et al.*, 1987; *Ingram et al.*, 1989; *Moritz et al.*, 1993; *Jin et al.*, 1994; *Rind et al.*, 1995; *Battisti et al.*, 1997]. This combination of potential importance and limited understanding provided the motivation for a large interdisciplinary study called the Surface Heat Budget of the Arctic Ocean (SHEBA).

[3] The primary goals of SHEBA are (1) to determine the ice-ocean-atmosphere processes that control the ice-albedo and cloud radiation feedback mechanisms and (2) to develop models that improve simulations of Arctic climate in general circulation models [*Moritz et al.*, 1993; *Moritz and Perovich*, 1996]. A central component of SHEBA was a yearlong field experiment from October 1997 through October 1998 [*Perovich et al.*, 1999a] directed at acquiring a high-quality, comprehensive, integrated data set that defined the state of the atmosphere, ice, and ocean over an entire annual cycle. Since the ice is, in essence, a grand integrator of the heat budget at the surface and bottom of the ice, an extensive program of mass balance measurements was an integral part of SHEBA. The mass balance programs included observations of growth on the bottom of the ice and ablation on both the ice surface and bottom.

[1]Engineer Research and Development Center, Cold Regions Research and Engineering Laboratory, Hanover, New Hampshire, USA.
[2]Department of Atmospheric Sciences, University of Washington, Seattle, Washington, USA.
[3]Geophysical Institute, University of Alaska, Fairbanks, Alaska, USA.

0148-0227/03/2001JC001079

[4] Due, in large part, to the expense involved in operating a long-term field camp, there are few results from long-term sea ice mass balance studies. Previous work [*Untersteiner*, 1961; *Hanson*, 1965; *Koerner*, 1973; *Bilello*, 1980; *McPhee and Untersteiner*, 1982; *Wettlaufer*, 1991; *Maykut and McPhee*, 1995; *Lytle and Ackley*, 1996; *Perovich et al.*, 1997] indicates that there is significant spatial and interannual variability in the mass balance of the sea ice cover. Indeed, *Untersteiner* [1961] and *Hanson* [1965] suggest that the temporal variability between years at a particular location may be greater than the spatial variability in a single year at different sites. Based on a wealth of data from Russian drifting stations, *Romanov* [1995] has compiled maps of key ice mass balance parameters. Taking into consideration problems of publication language and access, we are not aware of published studies of the interannual or spatial variability of mass balance parameters. Nevertheless, a number of Russian papers are directly or indirectly concerned with related problems, and we suspect that there may be others [e.g., *Yanes*, 1962; *Nazintsev*, 1963; *Doronin and Kheisin*, 1977; *Makshtas*, 1991].

[5] During the SHEBA field experiment we monitored ice growth and decay at more than 100 sites over an annual cycle from October 1997 to October 1998. In this paper we discuss the mass balance measurement program, present ice mass balance and temperature results for multiyear ice, and examine the annual mass balance cycle for all sites. Simple relationships between snow depth and ice thickness, and ice growth and ice melt are explored. The roles of snow, ponds, ridges, and leads in the mass balance of the ice cover are discussed. Results from SHEBA are placed in the context of earlier mass balance studies. Finally, relationships between melt rates and environmental forcing are considered.

2. Instruments and Methods

[6] The Arctic sea ice cover is spatially variable, consisting of leads, first-year ice, and multiyear ice and of undeformed, ridged, and ponded ice. Ice thickness ranges from open water to ridges tens of meters thick, and snow depths vary from millimeters to more than a meter. To understand the mass balance of the ice cover, it is necessary to understand the mass balance of these components. Because of the inherent variability, the ice mass balance was monitored at 135 locations, encompassing first-year ice, ponded ice, unponded ice, multiyear ice, hummocks, new ridges, and old ridges. The initial ice thicknesses for these sites ranged from 0.3 to 8 m, and snow depths varied from a few centimeters to more than a meter.

[7] Measuring ice growth and decay was a decidedly low-tech operation. We used a combination of an ablation stake and a hot-wire thickness gauge (Figure 1). The ablation stake was a 3-m-long wooden stake, painted white and marked with metric tape. The stakes were typically installed with 1.5 m frozen in the ice and the other 1.5 m in the air. The surface position was measured off the stake to the nearest 0.5 cm. The snow depth was also measured at each stake. Adjacent to the ablation stake was a hot-wire thickness gauge, consisting of a stainless steel wire

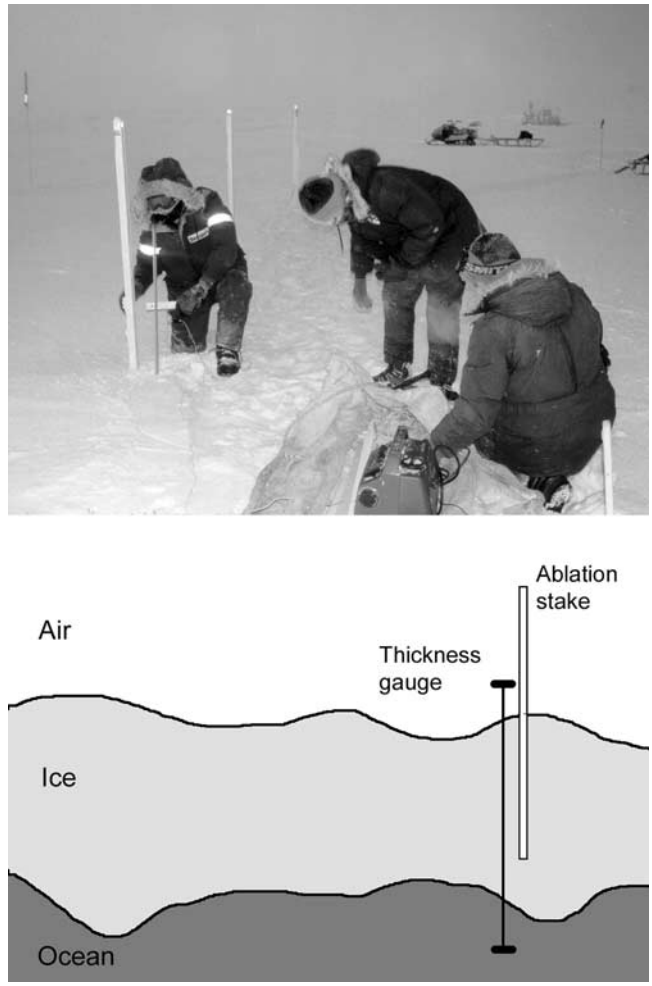

Figure 1. Photograph and schematic of a mass balance site. The instrumentation consists of an ablation stake and a thickness gauge. In the photograph one person is pulling up a thickness gauge.

with a steel rod attached as a crossbar on the bottom end and a wooden handle on the top end. To make a measurement the stainless steel wire was hooked to a generator that was also connected to a copper wire grounded in the ocean. The electrical resistance of the stainless steel wire melted it free, and the handle was pulled upward until the steel rod hit the bottom of the ice. The handle position was read off the ablation stake, giving the position of the ice bottom. Uncertainties of stake and gauge readings were typically less than 0.5 cm. In some cases, thickness gauges gave erratic readings because of ice blocks on the ice bottom. Mass balance measurements were made every 1–2 weeks during ice growth and every other day during the melt season. Most mass balance sites also had a thermistor string and datalogger measuring ice temperature profiles every hour [*Perovich and Elder*, 2002]. Over 100 mass balance gauges were installed in October 1997 at the beginning of the SHEBA field experiment. Additional gauges were installed in March, April, and June for a total of 135 gauges. Several of these gauges were lost during the year by being crushed in pressure ridges, frozen into the ice bottom, or melted free of the ice in summer. There were 93

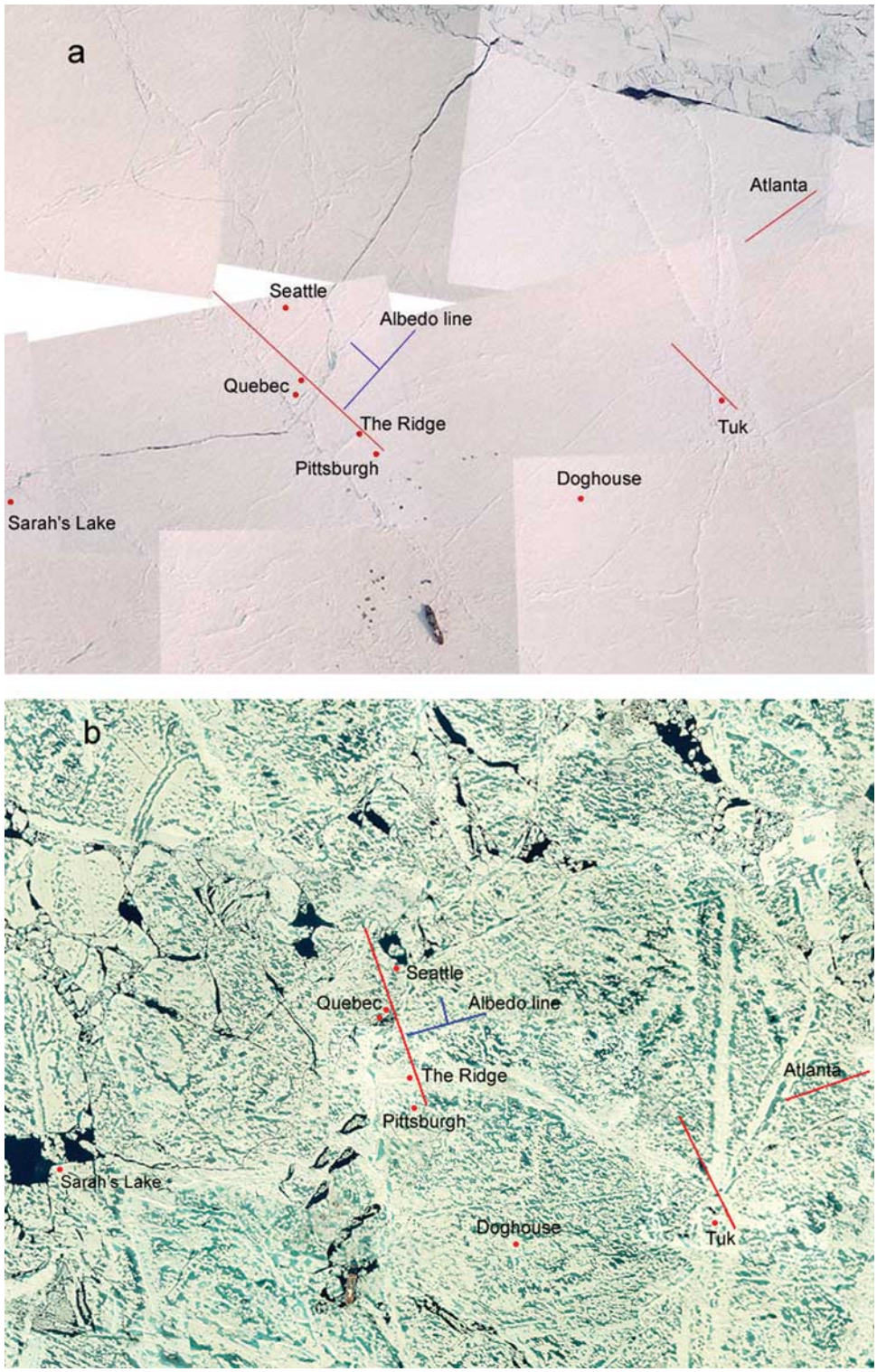

Figure 2. Aerial photomosaics of a 10 by 10 km area surrounding Ice Station SHEBA from (top) 17 May 1998 and (bottom) 25 July 1998. Note the profound change in surface conditions from snow covered ice to a mixture of bare ice, melt ponds, and leads.

stakes that lasted through the winter and 68 that lasted the entire year.

[8] The 135 gauges were grouped into 10 sites. Figure 2 shows the relative positions and names of these sites. It also provides a vivid example of the surface changes that occur during summer melt. On 17 May the surface was snow covered and uniform in appearance, with little open water. By 25 July extensive surface ablation had melted the snow cover and transformed the surface into a mixture of bare ice, melt ponds, and leads.

[9] Each of the ten mass balance sites had somewhat different properties (Table 1). The Pittsburgh mass balance

Table 1. Summary of Ice Mass Balance Sites[a]

Site	Gauges Installed	Yearlong Gauges	T String	Comments
Pittsburgh	5	4	yes	relative thick multiyear ice
The Ridge	20	14	yes	young ridge that probably formed in the spring of 1997
Quebec 1	7	1	yes	undeformed ice with an initial thickness of 0.85 cm
Quebec 2	4	3	yes	1.75-m-thick hummock
Seattle	29	10	yes	ponded area with nearby hummocks
Mainline	16	6	no	50-m-long line with undeformed and ponded multiyear ice
Tuk	22	17	yes	old consolidated ridge
Atlanta	10	6	no	45-m-long line with ponded and unponded multiyear ice
Doghouse	4	0	no	thick multiyear ice
Sarah's Lake	6	0	no	first-year ice with adjacent lead
Baltimore	12	7	yes	first-year ice with adjacent multiyear ice and a rubble zone

[a]Gauges is the number of thickness gauges at the site and T string denotes whether or not a thermistor string was installed at the site.

site was on relatively thick multiyear ice. Though surrounded by ponds, Pittsburgh remained a bare, white ice site throughout the summer. The Ridge mass balance site was a young ridge that probably formed in the spring of 1997. In the fall of 1997, individual blocks could easily be identified in the ridge sail and keel. The Quebec 1 and 2 mass balance sites were adjacent to each other. Quebec 1 was undeformed ice with an initial thickness of 0.85 m. Quebec 2 was a 1.75-m-thick hummock. In the fall of 1997 the Seattle mass balance site was a ponded area with nearby hummocks. Seattle was also heavily ponded in the summer of 1998. For the most part the ponded areas of 1997 were the ponded areas of 1998. The Mainline mass balance site was between Seattle and Quebec and consisted of a 50-m-long line of 16 ablation stakes spaced every 2.5 or 5 m. The line included undeformed and ponded multiyear ice. The Tuk mass balance site was an old consolidated ridge. There was significant ridging activity around Tuk throughout the winter of 1998. By spring it was partially surrounded by a ring of rubble. The Atlanta mass balance site consisted of 10 gauges in a line spaced every 5 m. The distribution of ice thickness along the Atlanta line was bimodal in the fall of 1997, with peaks at 0.84 and 1.44 m. There was evidence of ponding during the summer of 1997, and there was extensive ponding in this region during the summer of 1998. The Doghouse was a thick multiyear ice site with four thickness gauges and a water-level recorder. Sarah's Lake was a lead that developed in late May near the end of one of the runways. It was the location of an intensive observation program examining the thermohaline structure of a summer lead [*Pegau*, 2002; *Pegau and Paulson*, 2001; *Richter-Menge et al.*, 2002]. This first-year ice was about 1.7 m thick before melt began. This was relatively thick for first-year ice at SHEBA and was caused by a snow cover that was intentionally kept thin so that the ice could be used as a runway. The Baltimore mass balance site was first-year ice with adjacent multiyear ice and a transition rubble zone. Ice at this site started growing in late August 1997 and was about 40 cm thick in mid-October 1997. This area was heavily ponded in the summer of 1998, with many of the ponds melting all the way through to the ocean.

[10] Surface conditions before and after the onset of melt at Pittsburgh, Seattle, and the Mainline are displayed in Figure 3. The after-melt photographs illustrate the extensive ponding that developed during the SHEBA summer. The white stakes in the photographs are the ablation stakes with thickness gauges attached.

3. Results

3.1. Annual Cycle

[11] The annual cycle (October 1997 to October 1998) of temperature and mass balance for multiyear ice at the Quebec 2 site is plotted in Figure 4. The maximum snow depth at this site was about 12 cm, significantly less than the SHEBA average of 34 cm. The contours show the propagation of the fall freeze-up cold front through the ice, reaching the bottom in early November. Winter ice temperatures at this site were as low as $-25°C$, due in large part to the thin snow cover. There was a gradual warming of the ice in April, followed by a rapid warming in late May and early June as melt began and the penetrating solar irradiance increased. The ice was essentially isothermal at the freezing point for the remainder of the summer. Only in September did the ice begin to cool again. The annual cycle of ice temperature for ponded, ridged, and first-year ice is presented by *Perovich and Elder* [2002].

[12] At the Quebec multiyear site, ice growth started in November and continued until June (Figure 4b). The ice thickness at this site increased from 180 cm in October 1997 to 260 cm in June 1998. This was a relatively large amount of growth, caused by the thin snow cover. The growth rate increased during the fall, reaching a maximum of 0.8 cm per day in early January. Growth was fairly constant throughout the winter, then decreased in April and May. The growth rate at Quebec 2 averaged approximately 0.5 cm per day, overall. There was a brief period near the end of March when growth rates were negative, i.e., when there was bottom ablation of the ice. This was surprising, as the air temperature was about $-30°C$. The bottom melting was caused by a sharp increase in the ocean heat flux from a few W m^{-2} to values as large as 40 W m^{-2} [*Uttal et al.*, 2002; M. G. McPhee, personal communication, 2000]. The increase in ocean heat flux was caused by the entrainment of warmer, deeper water as a storm rapidly moved the ice station into shallower water on the Chukchi Cap. The entrainment of warm water was a short-lived phenomena, after which bottom growth resumed.

[13] A rainstorm on 29 May marked the beginning of the surface melt season. At this site the thin snow cover melted rapidly and was gone by 5 June. Surface melting continued until about 17 August, when fall freeze-up began. There

Figure 3. Photographs before (left) and after (right) melt at the Pittsburgh, Seattle, and Mainline mass balance sites. There was extensive ponding at all sites during summer.

was 75 cm of surface ablation at this site during the summer. There were a few 1- or 2-day periods during the summer when air temperatures cooled below freezing and there was a brief hiatus in surface melting. There were also a couple of light, ephemeral snowfalls in June; the new snow melted within a day or two. The surface melt rate averaged 1 cm day^{-1}, with a peak value of 4 cm day^{-1}. The surface melt season at SHEBA was long, lasting 80 days, compared to an average of 55 days reported from Russian drifting stations [*Serreze et al.*, 1997; *Lindsay*, 1998; *Perovich et al.*, 1999a].

[14] Bottom melt began in early June and continued throughout the summer, finally ending in early October. During this time there was 55 cm of bottom ablation. The bottom melt rate (Figure 4b) gradually increased during the summer, reaching a maximum during the first half of August and decreasing afterwards. The average melt rate was approximately 0.5 cm day^{-1}, with a peak value of nearly 1.5 cm day^{-1}.

[15] At the beginning of the SHEBA drift in October 1997, we were surprised at how thin the ice cover was [*McPhee et al.*, 1998; *Perovich et al.*, 1999a]. Submarine surveys, as well as ice thickness measurements indicated a mean ice thickness of approximately 150 cm and a median thickness of 90 cm. Because the ice was initially so thin [*McPhee et al.*, 1998] and there was a northward drift of 500 km [*Perovich et al.*, 1999a], we anticipated a net increase in ice thickness during the SHEBA year. This was not the case. The 180-cm ice plotted in Figure 4 grew 80 cm in winter but had 130 cm of melt during the summer, for a net loss of 50 cm. The thin ice grew thinner. However, Figure 4 presents results from only one site, which had undeformed multiyear

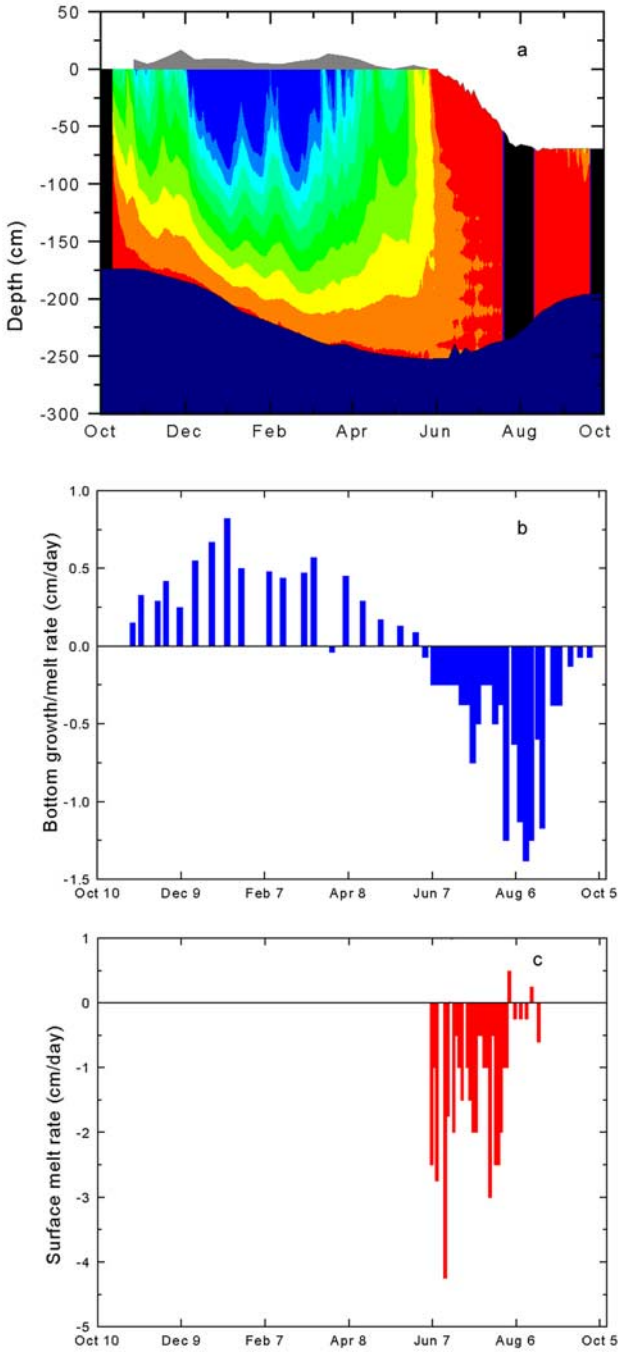

Figure 4. Annual cycle of (a) mass balance, (b) bottom growth rate and melt rate, and (c) surface melt rate for multiyear ice, using data from the Quebec site. In Figure 4a the internal ice temperature is displayed using color contours, with blue being cold (−20°C) and red, warm (0°C). The gray shaded area represents snow depth, and the black, missing data. The boundary between red and navy blue denotes the ice-ocean interface. In Figures 4b and 4c, positive melt rates mean growth and negative, melt.

ice with a thin snow cover. Was this site exceptional or was the thinning of the ice generally true?

[16] The change in ice thickness from October 1997 to October 1998 for 77 thickness gauges is plotted in Figure 5. The gauges are grouped into four categories based on the initial ice thickness: first-year ice, thin undeformed ice 0.7 to 1.5 m, thick undeformed ice 1.5 to 2.25 m, and deformed ice above 2.25 m. With the exception of a few ridge cases, the thicknesses followed a similar evolutionary pattern. There was a steady increase in thickness through the winter, a gradual tapering in the spring, a steep drop in thickness during summer melt, and another tapering in late summer and early fall. Ice growth was greatest for the first-year ice, and for a few of the thick ridge sites the ice thinned even in winter.

[17] The zero line in Figure 5 is the break-even line: points above the line represent a net increase in thickness; below, a net loss. Every site ended the year below the line, indicating a net thinning for the year. The net loss ranged from as little as 20 cm for a site with a 1-m-deep snow cover to as much as 180 cm for a 6-m-thick ridge. The average net loss was approximately 75 cm. This can be converted into an annual net heat (Q_i) using

$$Q_i = \rho_i \Delta H_i L_f = \left(900\ \mathrm{kg \cdot m^{-3}}\right)\left(.75\ \mathrm{m}\right)\left(.335\ \mathrm{MJ \cdot kg^{-1}}\right) = 226\ \mathrm{MJ \cdot m^{-2}} \quad (1)$$

and a net heat flux (F_{net}) using

$$F_{net} = \frac{Q_i}{\Delta t} = 7.2\ \mathrm{Wm^{-2}} \quad (2)$$

where ρ_i is the ice density, ΔH_i is the change in thickness, L_f is the latent heat of fusion of fresh ice, and Δt is the time interval of one year.

3.2. Total Growth and Melt

[18] A goal of the SHEBA program is to incorporate findings from the field program into large-scale sea ice and climate models. An important element of this effort is to simplify the complex and detailed results of the field experiment into a form suitable for treatment in large-scale models. Using results from the 135 thickness gauges, we investigated relationships between the annual changes in ice mass balance and basic parameters such as snow depth and initial ice thickness. Eight scattergrams are presented in Figure 6. Each point in a scattergram represents the results from a single mass balance site. In each case, only gauges with complete records were selected. Also included in each plot is the time interval considered, the number of gauges used in the analysis, and the correlation coefficient (R^2) for a linear relationship of the form y = ax + b.

[19] From an idealized perspective it is expected that thinner ice would have a steeper temperature gradient, a larger conductive flux, and more ice growth than thicker ice [*Maykut*, 1986]. Figure 6a plots total ice growth versus initial ice thickness (October 1997). There is a weak trend toward more growth for thinner ice, but the correlation is small ($R^2 = -0.55$) and the scatter considerable. The range of ice growth at a particular thickness was as much as 80 cm.

[20] While the initial ice thickness did have an effect, there were other variables affecting total ice growth. Snow depth also impacts ice growth. Since the thermal conductivity of snow is approximately an order of magnitude less than that of ice, snow depth can impact ice growth as much as ice thickness. To investigate the combined effects

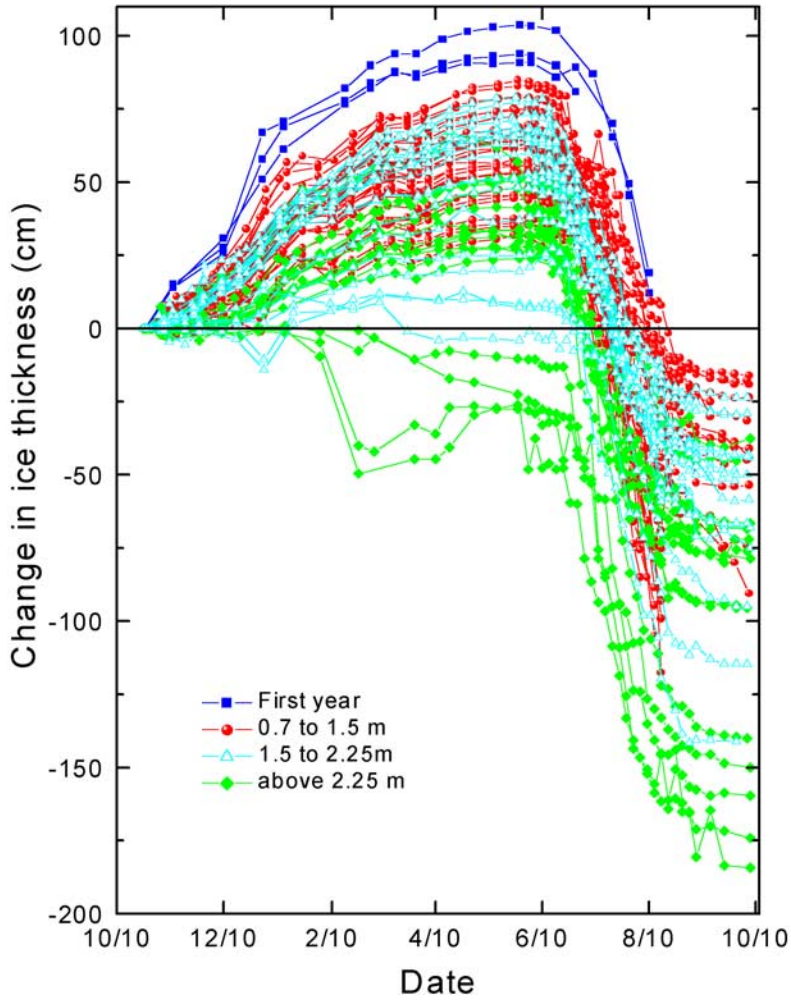

Figure 5. Annual cycle of change in ice thickness for 77 mass balance locations. The change in ice thickness relative to the initial thickness in October 1997 is plotted. The zero line is the break-even point. Above the line is a net increase in thickness and below is a net loss.

of initial ice thickness and snow depth, we defined an index H_{si}

$$H_{si} = H_i + H_s \frac{k_i}{k_s}, \tag{3}$$

where H_i is the initial ice thickness, H_s is the snow thickness, k_i is the ice conductivity of 2 W m^{-1} K^{-1} [*Yen et al.*, 1991], and k_s is the snow conductivity. *Sturm et al.* [2002a] state that SHEBA snow conductivities were in the 0.15- to 0.30-W m^{-1} K^{-1} range. For the present calculations we used a value of 0.3 W m^{-1} K^{-1}. A difficulty in using this index is determining a value for H_s. Because of blowing snow and precipitation, snow depths changed throughout the year [*Sturm et al.*, 2002b]. We selected snow depths measured at the beginning of January. This was after the autumn snowfall responsible for much of the snowpack and before the bulk of the ice growth. There is less scatter using the combined snow and ice index than when using only the ice thickness, and the correlation coefficient increased to −0.68 (Figure 6b).

[21] The mass balance data can also be used to explore ice melt relationships. Figure 6c is a scattergram plotting the snow depth in late May versus the date of the start of surface ice melt after all snow had melted. As expected, there was a connection between the two variables (R^2 = 0.66), with ice melt tending to start earlier at locations with a thinner snow cover. Much of the scatter in the plot resulted from the coarseness of the temporal resolution; surface ablation was only measured every other day.

[22] Since snow depth influenced the start of ice melt, it is reasonable to assume that snow depth also had an impact on the total amount of surface melt, with deeper snow related to less surface ice melt. However, Figure 6d indicates that this was not the case. There was only a weak relationship (R^2 = 0.17) between the snow depth and the amount of surface ice melt, and there was a considerable amount of scatter. For example, for the average snow depth of 34 cm, the amount of surface melt ranged from 50 to 110 cm. This variability was a direct result of different sites, each with the same amount of snow, following different evolutionary paths. The site with 50 cm of surface melt was a hummock, while the site with 110 cm of melt was a melt pond.

[23] We also determined that there was no relationship between the maximum ice thickness and the amount of

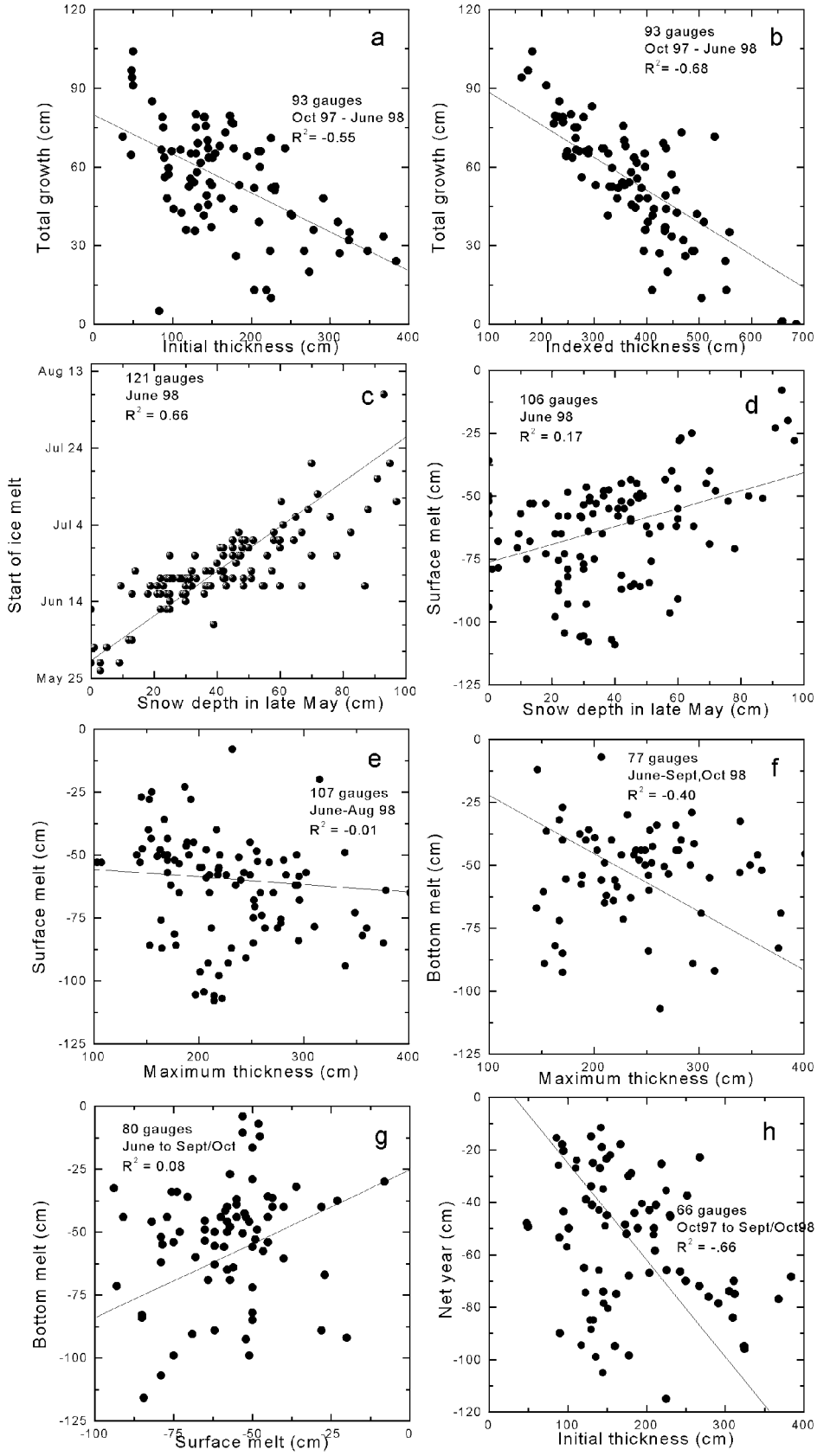
a
93 gauges
Oct 97 - June 98
R² = -0.55
Total growth (cm)
Initial thickness (cm)
b
93 gauges
Oct 97 - June 98
R² = -0.68
Total growth (cm)
Indexed thickness (cm)
c
121 gauges
June 98
R² = 0.66
Start of ice melt
Aug 13
Jul 24
Jul 4
Jun 14
May 25
Snow depth in late May (cm)
d
106 gauges
June 98
R² = 0.17
Surface melt (cm)
Snow depth in late May (cm)
e
107 gauges
June-Aug 98
R² = -0.01
Surface melt (cm)
Maximum thickness (cm)
f
77 gauges
June-Sept,Oct 98
R² = -0.40
Bottom melt (cm)
Maximum thickness (cm)
g
80 gauges
June to Sept/Oct
R² = 0.08
Bottom melt (cm)
Surface melt (cm)
h
66 gauges
Oct97 to Sept/Oct98
R² = -.66
Net year (cm)
Initial thickness (cm)

surface melt (Figure 6e). These two variables were uncorrelated ($R^2 = -0.01$). While there was a general increase in bottom melt with thickness (Figure 6f), the relationship was modest ($R^2 = -0.40$). For a given maximum thickness, the amount of bottom melting varied by as much as 75 cm. This implies that other factors in addition to thickness determine local variations in bottom melt. For instance, it is believed that ice bottom topography influences bottom melting [*Wettlaufer*, 1991; *McPhee*, 1992].

[24] There is no correlation ($R^2 = 0.08$) between the amounts of surface and bottom melt at a site (Figure 6g). The net loss for the year tended to be larger for thicker ice ($R^2 = -0.66$) (Figure 6h). There is considerable scatter in the data: for an initial ice thickness of 150 cm the net for the year ranged from −10 to −110 cm (Figure 6h). Many of the points show a linear trend, with bottom melt increasing with thickness. For large annual losses the data also appear to bifurcate as though there were two evolutionary paths that the ice could follow. For example, two locations with initial thicknesses of 90 and 320 cm both had a net annual loss 80 cm; one case was a melt pond and the other a ridge, showing that there are different paths to the same annual change in ice thickness. Conversely, different paths from the same starting point can lead to different net losses for the year. Studies of meltwater tracing showed that thinner ice was prone to collect under-ice meltwater that could enhance melt rates. At the same time, in some areas such under-ice melt layers can lead to false bottom formation, which to some extent buffers the ice against melt and hence can actually reduce bottom melt rates of thinner ice.

[25] The correlations in Figure 6 are somewhat disappointing. There do not appear to be simple relationships between, ice growth, ice melt, ice thickness, and snow depth. These parameters, as well as ice surface conditions and ice topography, all impact the growth and melt of the ice in a complex and interrelated manner. Paradoxically, we may be able to make some progress in generalizing the results by examining the data in less detail. Figure 7a is a histogram of total surface melt for the stakes highlighting results from ponded and unponded ice. There is a strong peak in the surface melt histogram with 30% of the cases falling in the 50–60 cm bin. Extending the range from 40 to 80 cm includes nearly 80% of all the mass balance gauges. Most of the gauges with more than 80 cm of melt were located in melt ponds. Unponded, bare ice had a mean surface melt of 56 cm and a standard deviation of 17 cm. Surface melt was greater for the ponded ice sites, where the mean was 78 cm and the standard deviation was 21 cm. This difference in surface melt was significant at the 99% confidence level.

[26] The distribution of bottom melt also exhibits a peak (Figure 7b), with 27% of the gauges having 40–50 cm of bottom melt and 70% in the 30- to 70-cm range. Approximately 13% of the gauges had more than 1 m of bottom ablation, all of which were in deformed ice. The difference in bottom melting between deformed and undeformed ice was statistically significant at the 99% confidence level. The deformed ice locations had a mean bottom melt of 76 cm and a standard deviation of 51 cm, compared to a mean of 48 cm and a standard deviation of 17 cm for the undeformed locations. This simple analysis confirms that for the SHEBA year, ponded ice had more surface melt than unponded ice and that deformed ice had more bottom melt than undeformed ice. It also indicates that a substantial fraction of the locations had similar amounts of surface melting and that many also had similar amounts of bottom melting.

3.3. Growth and Melt Rates

[27] Ice growth and melt rates were calculated by computing the first derivatives of the curves in Figure 5. These rates are directly related to the net heat flux of the ice. Growth rate time series for thin undeformed multiyear ice, thick undeformed multiyear ice, ponded ice, ridged ice, and first-year ice are plotted in Figure 8. The growth rate (f) was computed using

$$f = \frac{H_i(t_{j+1}) - H_i(t_j)}{t_{j+1} - t_j} \tag{4}$$

where H_i is the ice thickness, t_j is the time of one measurement, and t_{j+1} is time of the next measurement. All five groups followed the same general behavior, exhibiting peak growth rates of 0.3–1.3 cm day^{-1} in late December through mid-January followed by a gradual tapering the remainder of the winter. As with the example presented in Figure 4, all groups showed bottom melting at the end of March because of the warm water upwelling associated with drifting onto the Chukchi Cap. The old ridge had the smallest growth rates throughout the growth season. Initially the first-year ice and the thin multiyear ice had the largest growth rates, but after 1 April there was little difference among the nonridged cases. Over the entire growth season from late October until the end of May, first-year ice had the largest average growth rate (0.44 cm day^{-1}), followed by thin multiyear ice (0.35 cm day^{-1}), multiyear ice (0.30 cm day^{-1}), ponded ice (0.23 cm day^{-1}), and an old ridge (0.15 cm day^{-1}). Two factors contributed to the small growth rates of the ponded ice: freezing the pond's meltwater in the fall and the thicker snow cover found on frozen ponds.

[28] Surface and bottom melt rates averaged for all sites are plotted in Figure 9. Surface ablation of ice and snow was measured every other day, and bottom ablation was measured every fourth day. A three-point running mean was used to smooth the surface melt rate data. There was little surface ice melt at first because snow was melting. Ice equivalent snowmelt rates were calculated by multiplying the snowmelt rate by the ratio of the snow density (0.34 g cm^{-3}) to the ice density (0.9 g cm^{-3}). Ice equivalent snowmelt rates were approximately 0.5 cm day^{-1} for much of June. There

Figure 6. (opposite) Scattergrams investigating relationships between snow depth, ice thickness, snowmelt, surface melt, and bottom melt: (a) initial thickness versus total growth, (b) indexed thickness versus total growth, (c) snow depth prior to melt onset versus start of ice melt, (d) maximum snow depth versus total surface melt, (e) maximum ice thickness versus total surface melt, (f) maximum ice thickness versus total bottom melt, (g) total surface melt versus total bottom melt, and (h) initial ice thickness versus net change in thickness for the year.

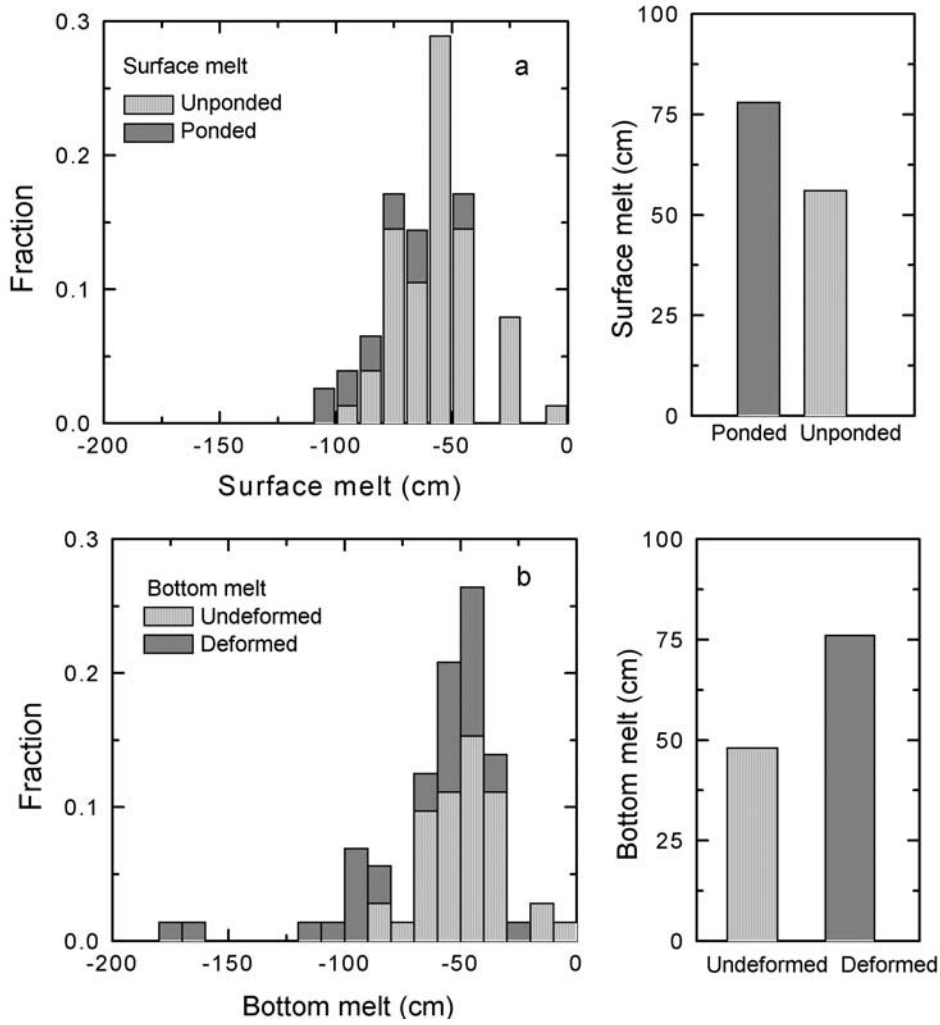

Figure 7. Histograms of the total amount of (a) surface melt and (b) bottom melt, along with comparisons of the average surface melt for ponded and unponded ice and the average bottom melt for deformed and undeformed ice.

was a gradual decrease starting on 23 June as the snow cover disappeared. By 13 June much of the snow was gone, and surface ice melt rate increased rapidly until 19 July, when a maximum value of 2.5 cm day^{-1} was reached. This is equivalent to a net surface heat flux of 75 W m^{-2}. The maximum was followed by a sharp and steady decrease in surface melt rate. Surface melt had ceased by the end of August. The average surface melt rate from 3 June to 27 August was 0.75 cm day^{-1}, equivalent to an average net surface flux of 26 W m^{-2}.

[29] The temporal evolution of the bottom melt rate curve was less striking than for the surface melt rate, and it was spread out over a longer period. The peak bottom melt rate of 1.2 cm day^{-1} was approximately half the surface value, and the rate of change of the bottom melt rate was more modest than for the surface melt rate. There was a slow, steady increase in bottom melt rate from 1 June to the peak on 30 July, followed by a steady decline until the end of the experiment. The net heat flux at the bottom of the ice during summer ranged from 10 to 40 W m^{-2}. The bottom melt rate peaked 11 days after the surface melt rate maximum. The average bottom melt rate from 3 June to 4 October was 0.50 cm day^{-1}, equivalent to an average net flux at the bottom of the ice of 17.5 W m^{-2}. While the maximum bottom melt rate was only half of the surface melt rate, bottom melting lasted a month longer than surface melting. Integrating the surface and bottom melt rate curves over time indicates that the total average surface melt (64 cm) and bottom melt (62 cm) were roughly comparable, and consequently so were the net heat inputs to the surface (193 MJ m^{-2}) and bottom (187 MJ m^{-2}).

[30] Surface and bottom ablation rates averaged for ponded ice, undeformed ice, and ridged ice are compared in Figure 10. First-year ice results were incomplete because all the thickness gauges in first-year ice melted free by early July. Surface melt rates were greatest for ponds. After the snow melted, ridge sails tended to have higher-than-average surface melt rates. Interestingly, ponds also tended to have the largest bottom melt rates from the end of July through August (Figure 10b). This was during and after the ice divergence event, when there was an overall increase in the bottom melt rate [*Richter-Menge et al.*, 2002]. We believe that during this active period, as the heat stored in leads was extracted by lateral and bottom melting, there was more

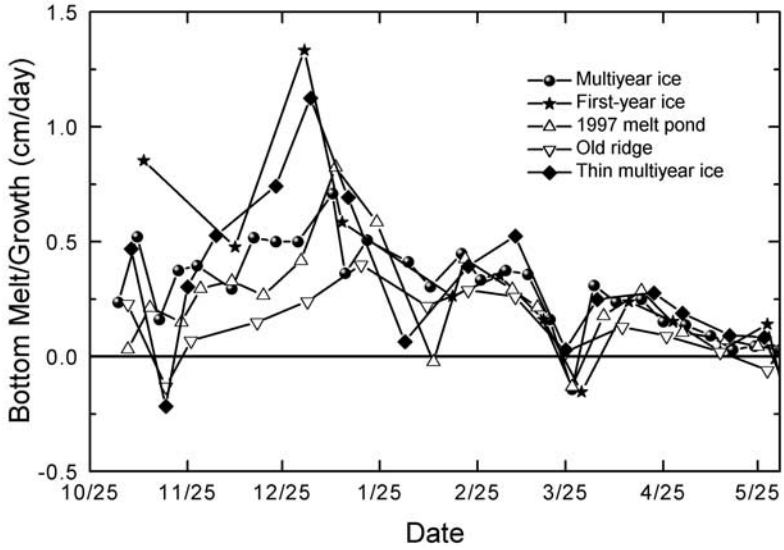

Figure 8. Time series of growth rates for multiyear ice, thin multiyear ice, first year ice, ponded ice, and ridged ice. A negative growth rate implies bottom melting.

bottom melting near the edges of floes than in the interior of the floe. After the dynamics-induced breakup, many of the pond gauges were near floe edges. We are uncertain if the enhanced bottom ablation for ponds was caused by enhanced penetration of solar radiation through ponds, related to the bottom topography of the pond, or merely a result of the pond sites being near floe edges. Ridge bottom melt rates were larger than the overall average for most of the year but were slightly less than average in August.

3.4. Snow Cover

[31] Snow has a significant impact on the mass balance of the ice cover in two opposing ways. During winter, snow thermally insulates the ice, reducing growth. In the summer, through its high albedo and its thermal mass, snow retards surface ablation of the ice. The importance of the snow for the mass balance motivated a detailed study of the temporal evolution and spatial variability of the snow cover in the vicinity of the SHEBA ice station [*Sturm et al.*, 2002a].

[32] From late August until the end of May there was a gradual buildup of the snowpack. Blowing snow was common during this period. By the end of May the mean snow depth was 34 cm, the median was 33 cm, and the average density was 0.34 g cm^{-3} [*Sturm et al.*, 2002a]. The snow cover exhibited considerable spatial variability, with depths at the thickness gauge locations ranging from 1 to 97 cm. High places, such as hummocks and ridge peaks, tended to have the thinnest snow cover. Melt ponds, being local depressions, accumulated snow earlier in the season and had deeper-than-average snow. The largest snow

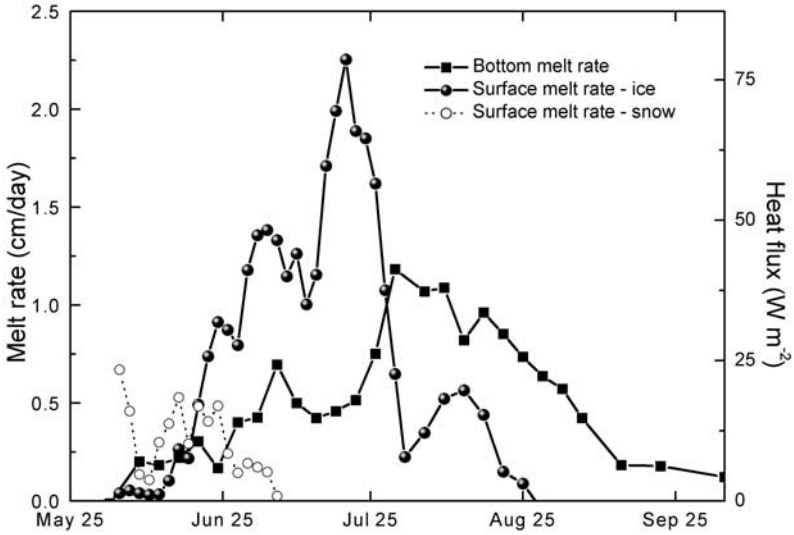

Figure 9. Time series of surface and bottom melt rates and the associated equivalent heat flux. The ice equivalent snowmelt rate is also plotted. For reference, the right axis provides the net heat flux equivalent to that melt rate, assuming an ice density of 0.9 g cm^{-3} and a latent heat of fusion of 335 J g^{-1}.

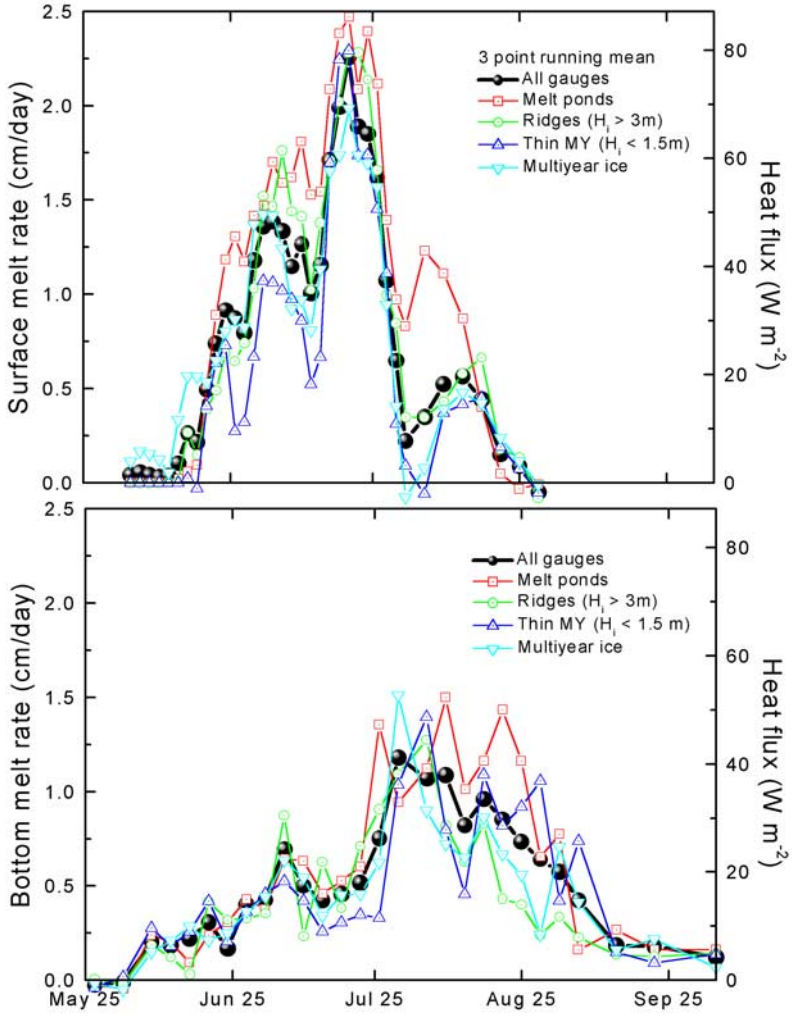

Figure 10. Time series of (top) surface and (bottom) bottom melt rates and the associated equivalent heat fluxes for ponded thin multiyear ice, multiyear ice, and ridges.

depths, about 1 m, were found in drifts that formed on the lee sides of ridges.

[33] Snowmelt was initiated at all the mass balance sites on 29 May by a rainstorm. Snowmelt proceeded rapidly, and by 30 June the average snow depth was only 3 cm. A few small snowdrift remnants lingered until the end of July. The total amount of heat per unit area needed to melt the snow cover was

$$Q_s = \rho_s H_s L_f = (340\ \mathrm{kg \cdot m^{-3}})(.34\ \mathrm{m})(.335\ \mathrm{MJ \cdot kg^{-1}}) = 38.7\ \mathrm{MJ \cdot m^{-2}} \quad (5)$$

For the period between 29 May and 24 June, when the average snow depth decreased from 0.34 to 0.05 m, an average contribution from the surface energy budget of 14.7 W m^{-2} was necessary to melt the snow.

3.5. Melt Ponds

[34] Melt ponds play a key role in the summer heat budget of sea ice. They reduce the albedo of the ice cover [*Perovich et al.*, 1999a], increase light transmittance to the ocean [*Grenfell and Maykut*, 1977], and serve as a storage reservoir for surface meltwater [*Eicken et al.*, 2002]. At Ice Station SHEBA, melt ponds began to form on the surface in mid-June in response to the snowmelt. As melt progressed, these ponds grew, both in area and in depth. Melt ponds were pervasive from June through August, covering over 20% of the surface during the height of the melt season in late July and early August. Throughout June and July and into the first half of August the ponds deepened, in some cases completely melting through to the ocean. Once a pond had a saltwater connection to the ocean, melting accelerated. Finally, by mid-August the pond surfaces began to freeze.

[35] There were two generic types of ponds at SHEBA: sea level ponds and "alpine" ponds [*Perovich et al.*, 1999b]. The sea level ponds were on undeformed ice, and the surfaces of the ponds were roughly at sea level during the latter half of the melt season [*Eicken et al.*, 2002]. The depth of these ponds tended to increase steadily throughout the summer as the pond bottom melted. The alpine ponds were located on the flanks of ridges, with the pond surface above sea level. Being above sea level the alpine ponds had a hydrostatic head, and their depths fluctuated depending on the balance between drainage and meltwater input. Sea level

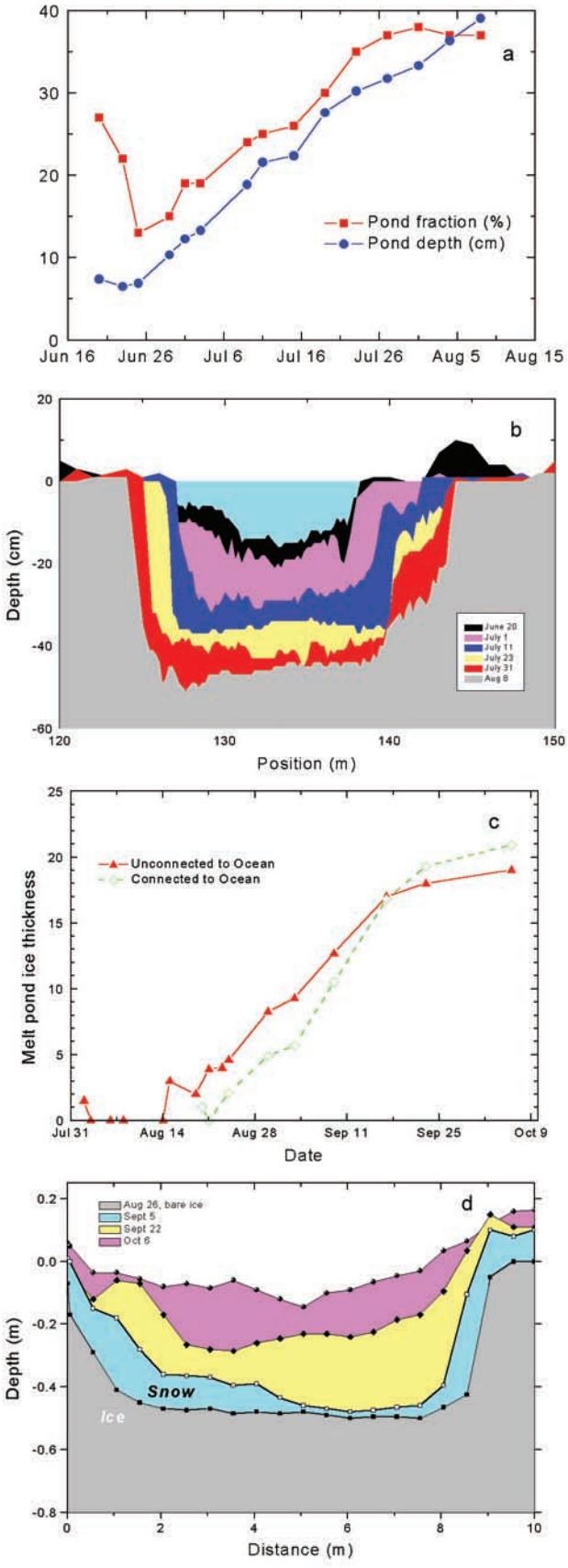

ponds were darker in appearance than alpine ponds and reflected less solar radiation [*Perovich et al.*, 1999a].

[36] The albedo of the ice cover is strongly influenced by the pond fraction [*Fetterer and Untersteiner*, 1998; *Perovich et al.*, 2002a]. Because of this importance, pond fractions were determined by analyzing aerial photographs [*Tschudi et al.*, 1997, 2002; *Perovich et al.*, 2002b]. As part of the mass balance program, we measured pond extent and depth along the 200-m-long albedo survey line every four days from mid-June through mid-August [*Perovich et al.*, 2002a]. The pond fraction along this line decreased at first as the ice became permeable and ponds drained, then steadily increased over the remainder of the summer, reaching a peak value near 40% in early August (Figure 11a). Peak pond fractions of the general SHEBA area determined from aerial photography were 24% [*Perovich et al.*, 2002b]. The ponds along the albedo line were all sea level ponds, and the average depth increased throughout the summer, reaching a maximum average depth of 40 cm in early August.

[37] Figure 11b shows the temporal evolution of a single pond along the survey line. The water surface of the pond is zero on the y axis and the color bands denote changes in pond width and depth. By the end of the summer this pond grew to about 0.5 m deep and 20 m wide. The widening of this pond was asymmetric, with increases of 3 m on the west side of the pond and 6 m on the east side. We do not have enough data to determine if asymmetric pond widening was common. The overall summer increase in pond fraction observed in the aerial photographs was probably a result of the preponderance of sea level ponds.

[38] Melt ponds began to freeze over in mid-August (Figure 11c). Ice growth started later in the ponds that had visible holes connecting them to the ocean because the ocean heat flux and the high water salinity inhibited growth. There was a slow, steady, linear increase in the thickness of the newly frozen surface layer, which reached a thickness of 20 cm after a month of growth. This corresponds to a latent heat release of about 54 MJ m^{-2}, equivalent to an average heat flux of 11 W m^{-2}. Shortly after the surface ice layer formed, snow covered the ponds. Since melt ponds are local depressions, drifting snow tended to accumulate rapidly. Figure 11d shows the buildup of snow from 26 August to 6 October in a melt pond. Even though there was only about 5–10 cm of snowfall during this period, the pond completely filled in with snow, resulting in pond snow depths of 40–50 cm. The combination of a deep snow cover and the meltwater in the pond significantly retarded growth on the bottom of the ice. The meltwater in the ponds that were measured had not yet completely frozen by the end of the field experiment in October 1998.

3.6. False Bottoms

[39] During the melt season, under special circumstances, lenses of ice can form at the underside of the ice [*Unter-*

Figure 11. (opposite) Evolution of melt ponds: (a) time series of the pond fraction and depth measured along a 200-m-long line; (b) widening and deepening of a single pond from 20 June through 8 August; (c) time series of ice freezing on the pond surface; (d) drifting of snow onto a frozen pond from 26 August through 6 October.

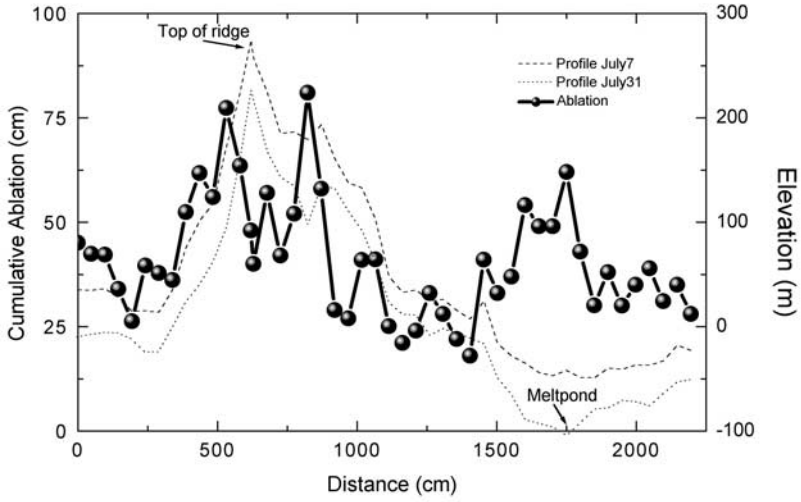

Figure 12. Surface ablation on a ridge sail, showing east-west profiles across the crest of a north-south ridge measured on 7 and 31 July and the profile of surface ablation during this period.

steiner, 1961; *Hanson*, 1965; *Eicken*, 1994; *Eicken et al.*, 1995]. These "false bottoms" result from double diffusive processes [*Martin and Kauffman*, 1974], where heat diffuses 100 times faster than salt in water. Fresh meltwater, near 0°C, drains from the ice and rests atop −1.6°C saline ocean water. Heat is quickly extracted from the meltwater, causing ice to form. Three conditions are needed for false bottom formation: (1) an input of fresh meltwater, (2) quiescent conditions to minimize mixing in the water column, and (3) a bottom topography that traps the fresh water.

[40] The impact of these false bottoms on the overall mass balance of the ice cover is probably small, but they do affect the input of fresh meltwater into the ocean [*Eicken*, 1994; *Eicken et al.*, 2002]. Determining the areal coverage of false bottoms is difficult, since they are on the underside of the ice and they are transient. However, the thickness gauges are also false bottom detectors, where apparent rapid ice growth in summer denotes the formation of a false bottom.

[41] Approximately 15% of the gauges showed false bottoms. These gauges tended to be in thinner ice and were often spatially clustered. For example, one prime location for false bottoms was at the Seattle location, an area that was ponded in the summer of 1997 and again in 1998. There were two major periods of false bottom production: around 7 June and in late July. The 7 June period was caused by the first surge of meltwater associated with the onset of snowmelt. We believe that the second period in late July occurred when the buildup of freshwater in leads extended below the ice bottom [*Richter-Menge et al.*, 2002]. The false bottoms tended to be short-lived, forming quickly and then melting in a few days to a week. They typically were located 10–20 cm below the bottom of the ice.

3.7. Ridges

[42] It has long been believed that ridge keels are sites of enhanced ocean heat exchange and preferential bottom melting. This was confirmed by this study (Figures 5 and 10). As Figure 10 indicates, bottom melt rates were consistently higher for deformed ice than for undeformed ice. The average cumulative bottom ablation for deformed ice was 80 cm, compared to 50 cm for undeformed ice. This difference was due, in part, to a few deep keels extending down more than 4 m that were melting the entire year (Figure 5).

[43] Melting on ridge sails is an interesting and complex problem. From a qualitative perspective, ice morphology indicates that there is enhanced melting on ridge sails. The sharp, well-defined sails of young ridges evolve into the rounded undulations of old sails. However, deep snow drifts often form on the flanks of ridges, reducing the amount of ice surface ablation. To investigate ablation on a young ridge sail, we installed a 22-m-long survey line across the summit of a 3-m-tall ridge. The survey line consisted of ablation stakes frozen into the ice with a rope suspended across the top of the stakes as a reference. Profiles of surface ablation were determined by measuring the distance to the surface every 50 cm along the rope. The ridge was oriented in a north-south direction, and the line was placed east-west perpendicular to the long axis of the ridge. Elevation profiles measured across the ridge on 7 and 31 July are plotted in Figure 12, along with profiles of total surface ablation during this period. Before melting began, the sail was approximately 3 m tall and 10 m wide, with a subduction zone on one side that was below sea level. The maximum ablation of 75 cm occurred on the upper flanks of the ridge. Meltwater collected into the subduction zone, forming a melt pond. There was 60 cm of surface melt in the ponded area. For comparison, the average surface ablation measured at the mass balance sites was 35 cm during this period. Even in summer, solar incident angles are small. The tilt of the ridge flanks resulted in a local enhancement of the solar radiation flux and consequently additional surface melt.

3.8. First-Year Ice

[44] Baltimore was the primary first-year ice site. This ice started growing at freeze-up in 1997 and was 40 cm thick by

the beginning of SHEBA in October. By the end of the growth season in late May, the average ice thickness and snow depth were 145 and 30 cm, respectively. The first-year ice had 45 cm of surface melt between 29 May and 30 July, when the last stake melted free. Ponding on the first-year ice at Baltimore was comparable, both in area and in depth, to that observed along the albedo line. However, since the ice was thinner, most of the first-year ponds melted through to the ocean. Unfortunately, all of the ablation stakes in the first-year ice melted free, so we do not have a complete record of the summer melt.

[45] In early February, ice divergence opened several leads in the vicinity of Ice Station SHEBA. We instrumented one of these freezing leads that was adjacent to the Quebec mass balance location. At the end of May the ice was slightly more that 1 m and had a rather thin 10-cm snow cover. By 4 July the ice had thinned to 43 cm and had deteriorated to a stage where further measurements were no longer possible. Within two weeks the ice had completely melted. In general, the first-year ice that formed in the winter or spring did not survive the summer melt season. Several factors contributed to this rapid and complete melt. The thin snow cover caused an early transition from snowmelt to ice melt. A lack of topography and freeboard led to a lack of meltwater drainage and a small albedo. In mid-June the albedo at the site was about 0.3 to 0.45, while the albedo of the adjacent multiyear ice was 0.6 to 0.7 [*Perovich et al.*, 2002a]. This smaller albedo allowed an additional 330 MJ m^{-2} to be deposited in the first-year ice or underlying water between the beginning of surface ice melt on 8 June and 4 July. This was enough energy to thin the ice by 110 cm, which by itself could account for the complete melting of the ice at this site. Also, once the ice thickness was less than about three-quarters of a meter, it was no longer optically thick. The albedo decreased further as the ice thinned, inputting more solar energy into the ice-ocean system and accelerating melting.

3.9. Lateral Melting

[46] Leads are dark and absorb 93% of the incident sunlight [*Pegau*, 2002]. Some of this absorbed energy contributes to lateral melting, and some is stored in the mixed layer. Most of it is ultimately used to thin the ice. To investigate this partitioning we measured lateral ablation and ice edge profile at 2- to 3-day intervals at floe edges at Seattle and Sarah's Lake (Figure 2b). Wave action in leads results in increased lateral heat transport and enhanced edge ablation at the waterline. This enhanced ablation can result in the formation of undercut overhangs of ice, as shown in Figure 13a for the Seattle lead. These overhangs extend as much as a few meters. Usually the cantilevered overhangs break off from the ice and then drift into the lead, where they rapidly melt. Beneath the waterline, wave action forms an ice shelf (Figure 13b). These shelves can protrude a few meters into the lead. The albedo of a shelf is similar to that of a melt pond. The combination of a small albedo and immersion in the lead cause accelerated melting of the shelves. The sequence of wall profiles in Figure 13c shows the temporal evolution of the ice edge. As the shelves melt, they often become honeycombed, creating more surface area for melting and weakening the ice and making it easier to break off the shelf should floes collide. The shelf pictured in Figure 13b did not break off, but it deteriorated during the second half of July, then rapidly melted as a storm in late July increased heat exchange between the lead and the ice [*Richter-Menge et al.*, 2002]. After this storm the 3-m-wide shelf was only 0.5 m wide. The total amount of lateral melting at this site was 4.3 m. Between 11 June and 17 August the average lateral melt rate at the Seattle lead was 6.4 cm day^{-1}, giving a temporally averaged lateral heat flux of 223 W m^{-2}. The Sarah's Lake site was adjacent to a different, larger lead approximately 1 km away from Seattle. The total amount of lateral melting at this location was 4.9 m, suggesting that lateral melting was somewhat similar, at least locally.

[47] The lateral melt rate and heat flux are almost an order of magnitude larger than the surface or bottom values. However, there is much more surface and bottom area than lateral area. The relative amounts of energy expended in surface (Q_s), bottom (Q_b), and lateral (Q_l) melting are illustrated by two examples in Table 2. One example was from 20 July, when the surface melt was near its maximum value, and the other was from 7 August, after a major ice divergence event [*Richter-Menge et al.*, 2002], when the bottom melt rate was large. For each case we determined the total heat expended for a square kilometer area using

$$Q_s = \rho_i L_f A_i f_s \Delta t \tag{6}$$

$$Q_b = \rho_i L_f A_i f_b \Delta t \tag{7}$$

$$Q_l = \rho_i L_f P H_i f_l \Delta t \tag{8}$$

where A_i is the ice area, P is the floe perimeter, and Δt is the time interval (one day). The average surface and bottom melt rates used are those presented in Figure 9. The ice area and perimeter were determined from an analysis of aerial photography [*Perovich et al.*, 2002b]. Values of H_i were determined by averaging thickness gauge results. On 20 July surface melting dominated, accounting for 77% of the heat expended in melting. The contribution from lateral melting was small, only 5%. By 7 August the distribution had changed. Bottom melting dominated (49%), with a substantial contribution (29%) from lateral melting. The jump in the lateral melting contribution resulted from an increase in floe perimeter that occurred when the ice cover broke up and diverged in late July. These results demonstrate that the relative contributions from surface, bottom, and lateral melt to ice mass loss change over the course of the melt season. The total floe perimeter strongly influences the amount of ice lost to lateral melting [*Maykut and Perovich*, 1987; *Steele*, 1992].

4. Discussion

[48] Given recent reports of Arctic warming, decreasing sea ice extent, and decreasing thickness [e.g., *Chapman and Walsh*, 1993; *Johannessen et al.*, 1995; *Cavalieri et al.*, 1997; *Parkinson et al.*, 1999; *Rothrock et al.*, 1999], it is of interest to this study to attempt to assess how the SHEBA drift experiment fits into the context of climatological ice conditions. *McPhee et al.* [1998] reported that the ice was

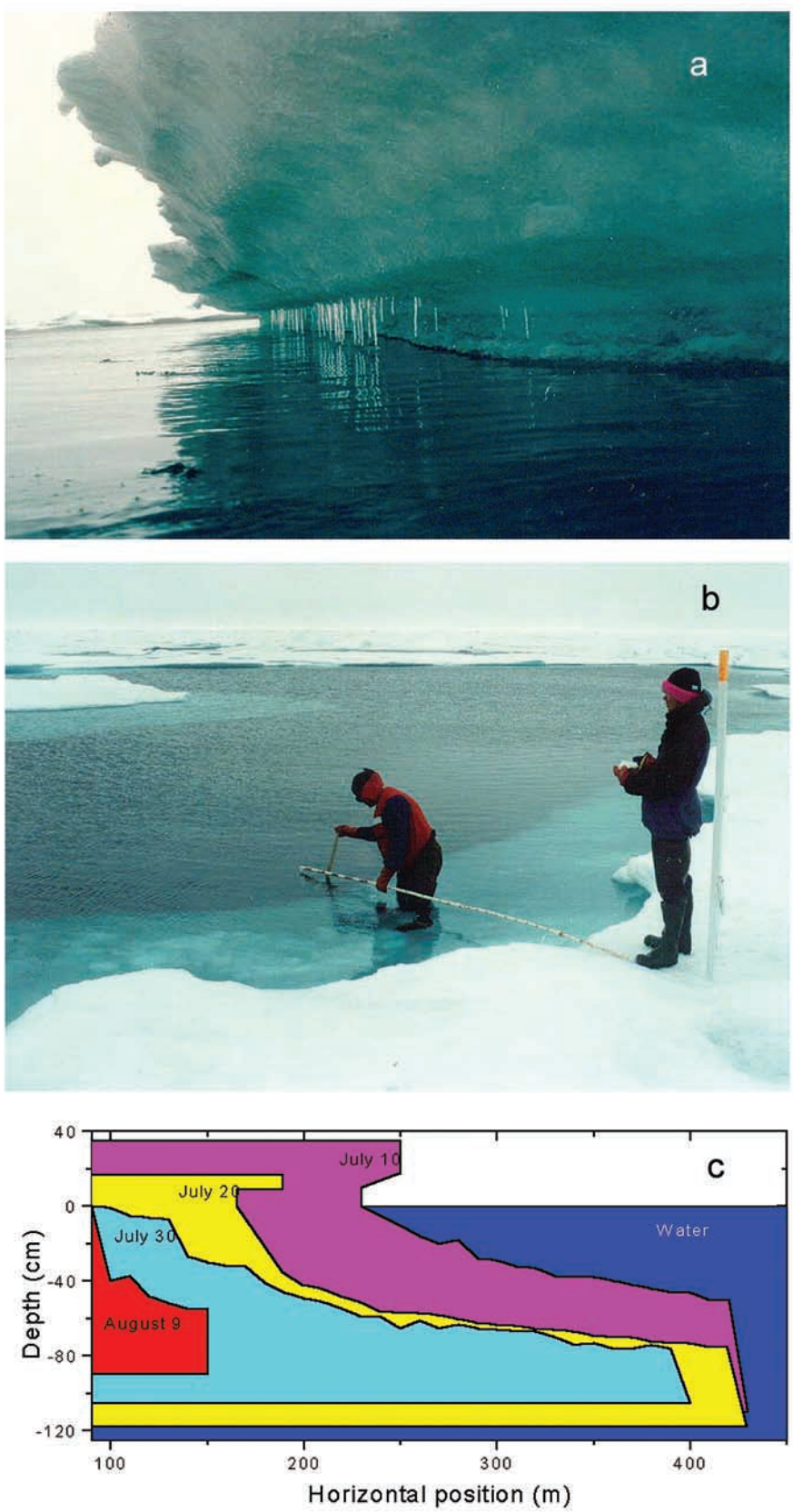

Figure 13. Lateral ablation of floe edges: (a) undercut ice, (b) an ice shelf, and (c) wall profiles showing lateral melt between 10 July and 5 August. The height of the hanging ice shelf featured in Figure 13a was approximately 20 cm.

Table 2. Comparison of Energy Expended in Surface, Bottom, and Lateral Melting, Before and After an Ice Divergence Event

Date	Latitude, N	Longitude, W	Ice Fraction	Lead Fraction	Pond Fraction	Floe Perimeter, km km^{-2}	Average Ice Thickness, m	Surface Melt Rate, cm day^{-1}	Bottom Melt Rate, cm day^{-1}	Lateral Melt Rate, cm day^{-1}	Q_s, GJ km^{-2}	Q_b, GJ km^{-2}	Q_l, GJ km^{-2}	Q_s, %	Q_b, %	Q_l, %
20-Jul-98	78 15.9	165 56.3	0.744	0.053	0.202	13.2	1.9	2.1	0.5	5.4	5990	1430	410	77	18	5
7-Aug-98	78 29.0	158 49.5	0.621	0.185	0.194	45.0	1.6	0.5	1.1	7.4	1230	2700	1610	22	49	29

anomalously thin in the area of the deployment of the SHEBA camp in October 1997. The camp was deployed at approximately 75°N, 143°W, thought to be the approximate center of the Beaufort Gyre, the persistent anticyclonic feature of ice and upper ocean circulation in the Canada Basin, which typically contains large concentrations of old, thick multiyear ice [*McPhee et al.*, 1998]. *McPhee et al.* [1998] and *Perovich et al.* [1999a] were impressed by the lack of thick ice, having anticipated that the mean thickness would range from 2 to 3 m. Indeed, the modal ice thickness for the region surrounding SHEBA was confirmed by a U.S. Navy submarine survey to be 0.9 m, with a mean thickness of 1.5 m. The thin ice and the finding that the upper ocean was warmer and less saline than measurements made two decades earlier [*McPhee et al.*, 1998] led to speculation that an unusual amount of melting had occurred in the summer of 1997.

[49] *Maslanik et al.* [1999] report that in 1998 the ice cover in the Beaufort and Chukchi Seas was at a record minimum extent for the period of record, 1953–1998. Based on records maintained by the National Ice Center, the distance northward from Point Barrow, Alaska, to the 50% ice concentration line for 15 September was the greatest ever observed (400 km) in 1998 for the 46 years of record; in 1997 it was the eighth largest. *Maslanik et al.* [1999] believe that the record reduction in 1998 occurred because of preconditioning by a light ice year in 1997 and atmospheric circulation patterns that generated predominately southerly and easterly winds. Nonetheless, *Perovich et al.* [1999a] point out that, from the measurements of surface air temperature made during the SHEBA year (2 October 1997 through 11 October 1998), the SHEBA station was cooler than the 1979 to 1996 climatology by 0.6°C. The station experienced a cooler winter, but the melt season during 1998 was relatively long, approximately 80 days compared to an average of 55 days observed at Russian drifting ice stations [*Lindsay*, 1998]. The SHEBA experiment was deployed in thinner ice than would be expected, experienced a typical winter growth season, and endured an unusually long melt season. The interplay between the minimum ice extent and the long melt season and large amount of bottom melt is unclear. It is possible that solar radiation absorbed by the large expanse of open water south of SHEBA caused a general warming that prolonged the summer melt season. This represents a potential positive feedback and is worthy of future investigation.

[50] The fact that the thin ice of October 1997 was even thinner in October 1998 was surprising, particularly since the ice station drifted from 75°N to 80°N. Spending the summer monitoring the decay of the ice pack made the thinning all the more vivid. Of course, global warming pronouncements cannot be made based on results from one location for one year. However, the magnitude of the loss was remarkable: a net decrease of 75 cm in only one year. The combination of two consecutive, long melt seasons of 1997 and 1998 was evidenced in the record minimum ice extent in the Beaufort Sea in the autumn of 1998 [*Maslanik et al.*, 1999] and the thin ice in the SHEBA area. What if there were a third long melt season? The demise of the first-year ice provides a cautionary tale. The survival of bare ice depends on the persistence of a drained surface scattering layer that maintains a large albedo [*Perovich et al.*, 2002a]. For ponded ice the key is for the ice to be thick enough at the beginning of melt so that the pond doesn't melt through to the ocean. For ice less than 100 to 120 cm thick at the start of the SHEBA summer, neither of these conditions was satisfied. Also, thinner ice results in more of the pond coverage being sea level ponds, which increase in depth and area throughout the summer. A third year of extensive melt at the SHEBA site could have melted all but the ridged ice.

[51] Mass balance results from summer melt season experiments are summarized in Table 3. These measurements were made in different years and at different places, primarily in the western Arctic. The amount of melting exhibits considerable variability, with the total surface melt ranging from 17 to 67 cm and the bottom melt from 11 to 62 cm. The 1959 data reported by *Hanson* [1965] are from a location similar to SHEBA, but they differ greatly. The surface melt was 38 cm in 1959, compared to 56 cm at SHEBA. The greatest difference was in the amount of bottom ablation: 11 cm in 1959 and 62 cm during SHEBA, a six-fold increase. The SHEBA bottom melt is striking. Compared to the other cases in Table 3 it is the greatest bottom melt by almost a factor of two. Some of this difference may be due to the inclusion of deformed sites in determining the average bottom melt at SHEBA, but even if we only consider undeformed ice, the average bottom melt of 48 cm is still much larger than any other case.

[52] The time series of average surface and bottom melt rates (Figure 9) are, in essence, the net surface and bottom heat budget. It should be possible to relate the melt rates to the environmental forcing and gain insight into the causes of the extensive SHEBA melting. In a broad sense we believe that solar radiation drives the summer melt season, so we would expect the surface melt rate to be related to the net incident solar radiation. Figure 14 plots time series of net solar radiation and average surface melt rate. There is no strong correlation between the two curves. The net solar radiation peak was on 22 June, while the melt rate peak was one month later. In July the net solar radiation is decreasing, even as the melt rate is increasing. While the net solar radiation contributes to surface melt, other terms in the surface heat budget must also play a significant role. A more detailed analysis is needed that includes the long-wave and turbulent fluxes. Of particular interest is the role of clouds on surface melt. Our qualitative impression is that there was more surface melt on cloudy and foggy days than

Table 3. Comparison of Summer Melt From Various Years and Locations

Reference	Year	July Location		H_s	H_i	Start of Snow Melt	Start of Surface Ice Melt	Start of Bottom Melt	End of Surface Ice Melt	End of Bottom Melt	Snow Melt, [a] cm	Ice Surface Melt, cm	Pond Surface Melt, cm	Ice Bottom Melt, cm
		Latitude	Longitude											
Untersteiner [1961]	1957	82 N	165 W	39	300	mid-June	early July	early July	late July	October	14	17	34	24
Untersteiner [1961]	1958	84 N	145 W	37	316	mid-June	early July	early July	mid-Aug	October	14	30	94	26
Hanson [1965]	1959	77 N	163 W	28	290	2 Jun	17 Jun	n.a	n.a	n.a	10	38	98	11
Maykut and McPhee [1995]	1975	75 N	142 W		280	n.a	n.a	15 Jun	mid-Sept	mid-Sept	n.a	26	n.a	34
Perovich et al. [1997]	1994	75 N	158 W	35	258	8 Jun	14 Jun	mid-June	mid-Aug	mid-Sept	13	67	n.a	25
SHEBA	1998	78 N	165 W	34	220	29 May	mid-June	1 Jun	17 Aug	October	12	56	78	62

[a]Snow melt is expressed as ice equivalent, assuming a snow density of 0.33 and an ice density of 0.9; n.a., not available.

on sunny days during SHEBA. This enhanced melting may be due to an increase in the incoming long-wave radiation or to heat released as fog droplets condense on the surface. Further work is needed in this area.

[53] In general, the bottom melt rate is related to the heat content of the upper ocean and turbulent mixing in the boundary layer [*McPhee*, 1992]. Qualitatively, this appeared to be the case for bottom melt during SHEBA. Figure 15a plots the average bottom melt rate, along with the temperature elevation above freezing of the upper ocean [*Perovich et al.*, 1999a] and the floe speed. Simplifying greatly, we use the floe speed as a proxy for turbulent mixing. There was a steady increase in the heat content of the upper ocean from May through the beginning of August that mirrored the overall upward trend in bottom melt rate. The rapid increase in melt rate in early August is associated with the buildup of heat in the water plus a sharp jump in the floe speed. With the increase in bottom melt rate, heat was extracted from the ocean faster than it was input. The heat content of the upper ocean decreased, and so did the bottom melt rate. More work is needed to quantitatively describe heat transfer at the ice bottom.

[54] The greatest anomaly in the SHEBA year mass balance was the extraordinarily large amount of bottom melting. The average bottom melt was 62 cm, equivalent to 187 MJ m^{-2}. What was the source of this heat? *Maykut and McPhee* [1995] analyzed mass balance and oceanographic data from AIDJEX and determined that the energy source for the ocean heat flux was solar radiation penetrating into the upper ocean through leads. Leads have a small albedo [*Pegau and Paulson*, 2001] and act as windows, transmitting over 90% of the incident solar energy to the ocean. We estimated the solar energy through leads by combining observations of incident solar radiation (R. E. Moritz, personal communication, 1999), lead albedo [*Pegau*, 2002], and lead fraction [*Perovich et al*, 2002b]. Lead fractions were approximately 5% in June and July, increasing to 20% following a divergence event at the end of July. The results are plotted in Figure 15b, along with the cumulative heat used in bottom melting. The local solar energy input via leads accounts for only two-thirds of the observed bottom melting, so there must be a source of additional energy. There are both distant and local possible sources for the remainder of the energy. The heat could be advected from a distance; the summer ice edge was only roughly 100 km south of SHEBA, where there was ample energy input to the ocean. There may also have been a contribution from deeper, warmer waters, as was the case during the brief bottom melt event in March.

[55] Locally, solar energy was also transmitted to the ocean through ponds and through the ice. In the past these sources have been neglected, but with the extensive ponding and thin ice at Ice Station SHEBA, the contribution from ponds and ice may have been significant. A precise determination of this contribution is difficult, since light transmittance through ice varies both spatially and temporally. It depends not only on the fractional areas of ice and ponds but also on the temporal evolution of the snow depth, ice thickness, and the pond depth distributions. Using the observed fractional areas [*Perovich et al.*, 2002b], it is possible to generate a crude estimate of the snow-free transmittances for ice and ponds needed to generate the 60 MJ m^{-2} heat deficit. Transmittances of approximately 3% for bare ice and 15% for ponded ice would be sufficient. These estimates are unrefined but reasonable [*Grenfell and Maykut*, 1977] and suggest that transmittance through ice and ponds may make a significant contribution to solar heating of the upper ocean. A more detailed analysis of the energy source for bottom melting is needed.

[56] In spite of the importance of the mass balance of sea ice, there is a paucity of data. Long-term mass balance measurements are logistically demanding, and there haven't been many opportunities to conduct such studies. There is a large mass balance data set from Russian drifting stations that needs to be made available to the scientific community similar to the meteorological and snow data already available through the efforts of the *Environmental Working Group* [1997]. Long-term time series data from many different sites are needed to explore and understand the spatial and temporal variability of the mass balance. Drifting manned stations provide valuable data but are limited in areal and temporal extent. Satellites can provide large-scale information monitoring ice extent, as well as the onset of melt and freeze-up. Autonomous ice buoys can provide mass balance measurements equivalent to those presented in Figure 4 [*Peterson et al.*, 1991; *Perovich et al.*, 1997], which can be used in conjunction with models to estimate regional ice growth and melt. Repeated submarine-based surveys of ice thickness can provide large-scale information on the ice mass balance.

5. Conclusions

[57] The SHEBA winter was slightly colder than the long-term average, but the melt season of 1998 was longer. This led to substantial net thinning of the ice cover. The initially thin ice at Ice Station SHEBA had a net loss of 75 cm during the annual cycle from October 1997 to October

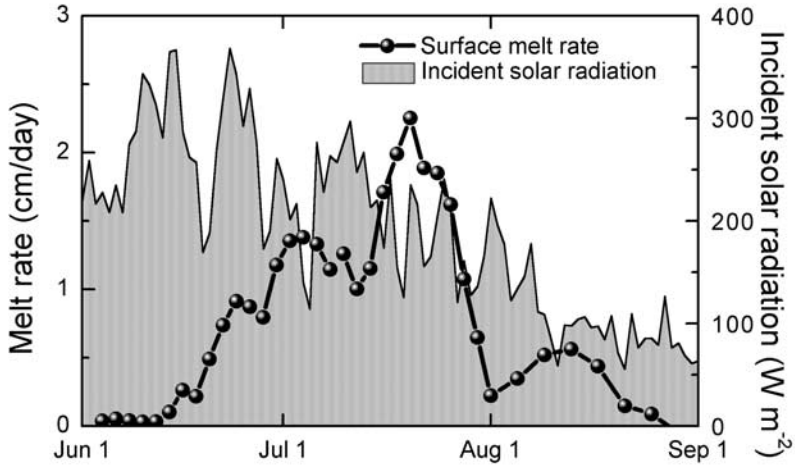

Figure 14. Time series of surface melt rate and net solar energy.

1998. The average bottom ablation of 62 cm at SHEBA was surprising large, more than twice the amount reported from previous experiments. Solar radiation input locally to the ocean through leads was not sufficient to account for the observed bottom ablation. Light transmitted through melt ponds, and even bare ice, may contribute substantially to solar heating of the upper ocean. The melt season was started by a rainstorm on 29 May. Peak melt rates were in

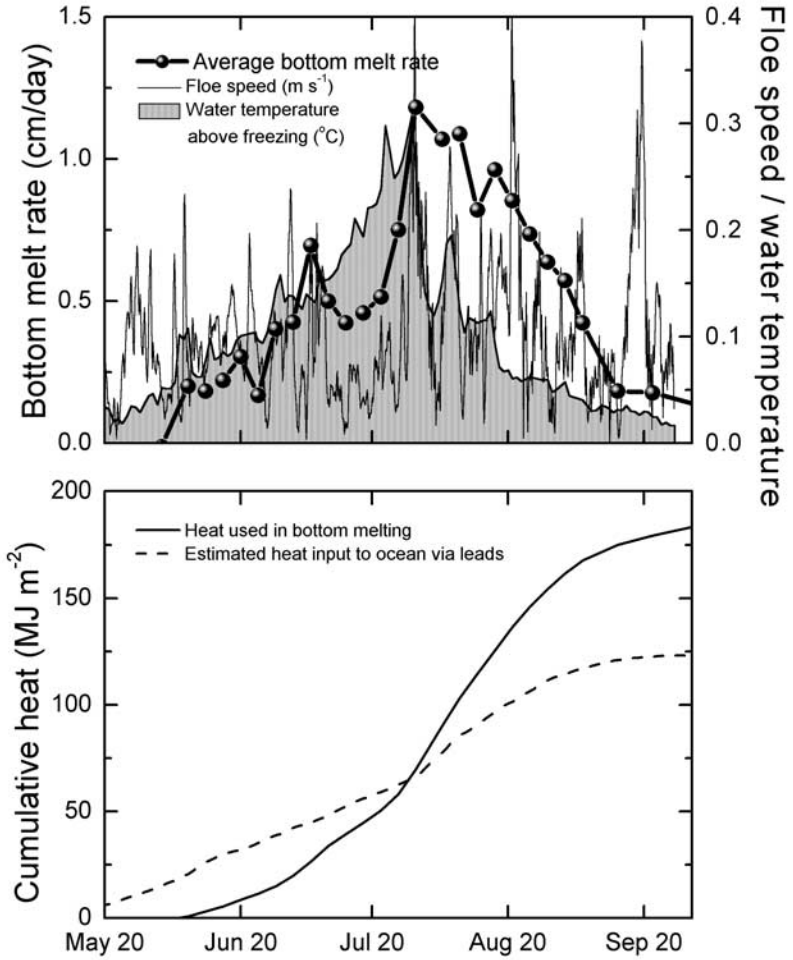

Figure 15. Time series of average bottom melt rate and associated parameters: (top) average bottom melt rate, water temperature above freezing, and floe speed; (bottom) heat used in bottom melting (solid line) and estimated heat input to the upper ocean through leads (dashed line).

mid-July for surface ablation, when low clouds and a warm air mass intruded over SHEBA. Bottom ablation peaked in early August, when there was a sharp increase in ice drift and divergence. Sea level melt ponds grew deeper and wider throughout the summer, resulting in a steady increase in pond coverage to a peak of 24%. Ponded ice exhibited the greatest surface melt, and deformed ice, the greatest bottom melt. Melt rates on floe edges were much higher than surface or bottom melt rates. However, since the relative area of ice edge was smaller than the surface or bottom area, lateral melting did not dominate the overall mass loss.

[58] Surface and bottom melt rates are presented and are qualitatively related to the atmospheric and ocean forcing. The next step is to integrate the mass balance results with other SHEBA observations to quantify these relationships. Of particular interest is determining the impact of clouds, long-wave radiation, and turbulent fluxes on surface melt and ascertaining the heat source for bottom melting. Once quantitative relationships are derived, they can be simplified and incorporated into large-scale sea ice models and general circulation models.

[59] **Acknowledgments.** The authors thank B. Elder, H. Bosworth, J. Govoni, K. Claffey, R. Belyea, and J. Ukita for their capable assistance in the field measurements. We also thank the crew of the *Des Groseilliers* and the SHEBA Logistics Office for their excellent support. SHEBA was sponsored by the National Science Foundation Office of Polar Programs and the Office of Naval Research High Latitude Physics Program. This work was funded under Office of Naval Research Grant N00014-97-1-0765.

References

Battisti, D. S., C. M. Bitz, and R. E. Moritz, Do general circulation models underestimate the natural variability in the Arctic climate?, *J. Clim.*, *10*, 1909–1920, 1997.

Bilello, M. A., Maximum thickness and subsequent decay of lake, river, and fast sea ice in Canada and Alaska, *CRREL Rep. 80-6*, 160 pp., Cold Reg. Res. and Eng. Lab., Hanover, N. H., 1980.

Cavalieri, D. J., P. Gloersen, C. L. Parkinson, J. C. Comiso, and H. J. Zwally, Observed hemispheric asymmetry in global sea ice changes, *Science*, *278*, 1104–1106, 1997.

Chapman, W. L., and J. E. Walsh, Recent variations of sea ice and air temperature in high latitudes, *Bull. Am. Meteorol. Soc.*, *74*, 33–47, 1993.

Dickinson, R. E., G. A. Meehl, and W. M. Washington, Ice-albedo feedback in a CO_2-doubling simulation, *Clim. Change*, *10*, 241–248, 1987.

Doronin, Y. P., and D. E. Kheisin, *Sea Ice*, Amerind Publ. Co., New Delhi, 1977.

Eicken, H., Structure of under-ice melt ponds in the central Arctic and their effect on the sea ice cover, *Limnol. Oceanogr.*, *39*, 682–694, 1994.

Eicken, H., M. Lensu, M. Lepparanta, W. B. Tucker III, A. J. Gow, and O. Salmela, Thickness, structure and properties of level summer multiyear ice in the Eurasian sector of the Arctic Ocean, *J. Geophys. Res.*, *100*, 22,697–22,710, 1995.

Eicken, H., H. R. Krouse, D. Kadko, and D. K. Perovich, Tracer studies of pathways and rates of meltwater transport through Arctic summer sea ice, *J. Geophys. Res.*, *107*(C10), 8046, doi:10.1029/2000JC000583, 2002.

Environmental Working Group, *Joint U.S. Russian Atlas of the Arctic Ocean—Oceanography Atlas for the Winter Period* [CD-ROM], Natl. Snow and Ice Data Cent., Boulder, Colo., 1997.

Fetterer, F., and N. Untersteiner, Observations of melt ponds on Arctic sea ice, *J. Geophys. Res.*, *103*, 24,821–24,835, 1998.

Grenfell, T. C., and G. A. Maykut, The optical properties of ice and snow in the Arctic Basin, *J. Glaciol.*, *18*, 445–463, 1977.

Hanson, A. M., Studies of the mass budget of Arctic ice pack floes, *J. Glaciol.*, *5*, 701–709, 1965.

Ingram, W. J., C. A. Wilson, and J. F. B. Mitchell, Modeling climate change: An assessment of sea ice and surface albedo feedbacks, *J. Geophys. Res.*, *94*, 8609–8622, 1989.

Jin, Z., K. Stamnes, and W. F. Weeks, The effect of sea ice on the solar energy budget in the atmosphere-sea ice-ocean system: A model study, *J. Geophys. Res.*, *99*(C12), 25,281–25,294, 1994.

Johannessen, O. M., M. Miles, and E. Bjorgo, The Arctic's shrinking sea ice, *Nature*, *376*, 126–127, 1995.

Koerner, R. M., The mass balance of the sea ice of the Arctic Ocean, *J. Glaciol.*, *12*, 173–185, 1973.

Lindsay, R. W., Temporal variability of the energy balance of thick Arctic pack ice, *J. Clim.*, *11*, 313–331, 1998.

Lytle, V. I., and S. F. Ackley, Heat flux through sea ice in the western Weddell Sea: Convective and conductive transfer processes, *J. Geophys. Res.*, *101*(C4), 8853–8868, 1996.

Makshtas, A. P., *The Heat Budget of Arctic Ice in the Winter*, Int. Glaciol. Soc., Cambridge, UK, 1991.

Martin, S., and P. Kauffman, The evolution of under-ice melt ponds, or double diffusion at the freezing point, *J. Fluid Mech.*, *64*, 507–527, 1974.

Maslanik, J. A., M. C. Serreze, and T. Agnew, On the record reduction in 1998 western arctic sea-ice cover, *Geophys. Res. Lett.*, *26*, 1905–1908, 1999.

Maykut, G. A., The surface heat and mass balance, *The Geophysics of Sea Ice*, edited by N. Untersteiner, 395–465, Plenum, New York, 1986.

Maykut, G. A., and M. G. McPhee, Solar heating of the Arctic mixed layer, *J. Geophys. Res.*, *100*, 24,691–24,703, 1995.

Maykut, G. A., and D. K. Perovich, On the role of shortwave radiation in the summer decay of a sea ice cover, *J. Geophys. Res.*, *92*(C7), 7032–7044, 1987.

McPhee, M. G., Turbulent heat flux in the upper ocean under sea ice, *J. Geophys. Res.*, *97*, 5365–5379, 1992.

McPhee, M. G., and N. Untersteiner, Using sea ice to measure vertical heat flux in the ocean, *J. Geophys. Res.*, *87*, 2071–2074, 1982.

McPhee, M. G., T. P. Stanton, J. H. Morison, and D. G. Martinson, Freshening of the upper ocean in the Arctic: Is perennial sea ice disappearing?, *Geophys. Res. Lett.*, *25*, 1729–1732, 1998.

Moritz, R. E., and D. K. Perovich (Eds.), *Surface Heat Budget of the Arctic Ocean, Science Plan*, *ARCSS/OAII Rep. 5*, 64 pp., Univ. of Wash., Seattle, 1996.

Moritz, R. E., J. A. Curry, A. S. Thorndike, and N. Untersteiner, *SHEBA, A Research Program on the Surface Heat Budget of the Arctic Ocean*, *Ocean Atmos. Ice Interac. Rep. 3*, 34 pp., Arc. Sys. Sci., Univ. of Wash., Seattle, Wash., 1993.

Nazintsev, Y. L., Role of thermal processes in ice melting and in modification of the relief of polar-ice floes in the central Arctic, *Probl. Arkt. Antarkt.*, *12*, 69–75, 1963.

Parkinson, C. L., D. J. Cavalieri, P. Gloersen, H. J. Zwally, and J. C. Comiso, Arctic sea ice extents, areas, and trends 1978–1996, *J. Geophys. Res.*, *104*, 20,837–20,856, 1999.

Pegau, W. S., Inherent optical properties of the central Arctic surface waters, *J. Geophys. Res.*, *107*(C10), 8035, doi:10.1029/2000JC000382, 2002.

Pegau, W. S., and C. A. Paulson, The albedo of Arctic leads in summer, *Ann. Glaciol.*, *33*, 221–224, 2001.

Perovich, D. K., and B. Elder, Estimates of ocean heat flux at SHEBA, *Geophys. Res. Lett.*, *29*(10), 1344, doi:10.1029/2001GL014171, 2002.

Perovich, D. K., B. C. Elder, and J. A. Richter-Menge, Observations of the annual cycle of sea ice temperature and mass balance, *Geophys. Res. Lett.*, *5*, 555–558, 1997.

Perovich, D. K., et al., Year on ice gives climate insights, *Eos Trans. AGU*, *80*, 481, 485–486, 1999a.

Perovich, D. K., T. C. Grenfell, B. Light, J. A. Richter-Menge, M. Sturm, W. B. Tucker III, H. Eicken, G. A. Maykut, and B. Elder, *SHEBA: Snow and Ice Studies* [CD-ROM], Cold. Reg. Res. and Eng. Lab., Hanover, N. H., Oct., 1999b.

Perovich, D. K., T. C. Grenfell, B. Light, and P. V. Hobbs, Seasonal evolution of the albedo of multiyear Arctic sea ice, *J. Geophys. Res.*, *107*(C10), 8044, doi:10.1029/2000JC000438, 2002a.

Perovich, D. K., W. B. Tucker III, and K. A. Ligett, Aerial observations of the evolution of ice surface conditions during summer, *J. Geophys. Res.*, *107*(C10), doi:10.1029/2000JC000449, 2002b.

Peterson, I., S. D. Smith, S. Prinsenberg, and R. H. Orton, Remote monitoring of thermal structure and growth of shore-fast ice off the Labrador coast, *Cold Reg. Sci. Technol.*, *19*, 123–130, 1991.

Richter-Menge, J. A., S. L. McNutt, J. E. Overland, and R. Kwok, Relating arctic pack ice stress and deformation under winter conditions, *J. Geophys. Res.*, *107*(C10), 8040, doi:10.1029/2000JC000477, 2002.

Rind, D., R. Healy, C. Parkinson, and D. Martinson, The role of sea ice in $2 \times CO2$ climate model sensitivity, I, The total influence of sea ice thickness and extent, *J.*, 450–463, 1995.

Romanov, I. P., *Atlas of Ice and Snow of the Arctic Basin and Siberian Shelf Seas*, 2nd ed., 277 pp., Backbone, New York, 1995.

Rothrock, D. A., Y. Yu, and G. A. Maykut, Thinning of the Arctic sea ice cover, *Geophys. Res. Lett.*, *26*, 3469–3472, 1999.

Serreze, M. C., J. A. Maslanik, J. R. Key, Atmospheric and sea ice characteristics of the Arctic Ocean and the SHEBA field region in the Beaufort Sea, *Spec. Rep. 4*, 219 pp., Natl. Snow and Ice Data Cent., Boulder, Colo., 1997.

Spelman, M. J., and S. Manabe, Influence of oceanic heat transport upon the sensitivity of a model climate, *J. Geophys. Res.*, *89*, 571–586, 1984.

Steele, M., Sea ice melting and floe geometry in a simple ice-ocean model, *J. Geophys. Res.*, *97*, 17,729–17,738, 1992.

Sturm, M., J. Holmgren, and D. K. Perovich, Winter snow cover on the sea ice of the Arctic Ocean at the Surface Heat Budget of the Arctic Ocean (SHEBA): Temporal evolution and spatial variability, *J. Geophys. Res.*, *107*(C10), 8047, doi:10.1029/2000JC000400, 2002a.

Sturm, M., D. K. Perovich, and J. Holmgren, Thermal conductivity and heat transfer through the snow on the ice of the Beaufort Sea, *J. Geophys. Res.*, *107*(C21), 8043, doi:10.1029/2000JC000409, 2002b.

Tschudi, M. A., J. A. Curry, and J. A. Maslanik, Determination of areal surface-feature coverage in the Beaufort Sea using aircraft video data, *Ann. Glaciol.*, *25*, 434–438, 1997.

Tschudi, M. A., J. A. Curry, and J. A. Maslanik, Characterization of springtime leads in the Beaufort/Chukchi Seas from airborne and satellite observations during FIRE/SHEBA, *J. Geophys. Res.*, *107*(C10), 8034, doi:10.1029/2000JC000541, 2002.

Untersteiner, N., On the mass and heat budget of Arctic sea ice, *Arch. Meteorol. Geophys. Bioklimatol., Ser. A*, *12*, 151–182, 1961.

Uttal, T., et al., Heat Budget of the Arctic Ocean, *Bull. Am. Meteorol. Soc.*, *83*, 255–275, 2002.

Washington, W., and G. Meehl, General circulation model CO_2 sensitivity experiments: Snow-sea ice albedo parameterizations and globally averaged surface air temperature, *Clim. Change*, *8*, 231–241, 1986.

Wettlaufer, J., Heat flux at the ice-ocean interface, *J. Geophys. Res.*, *96*, 7215–7236, 1991.

Yanes, A. V., Melting of snow and ice in the central Arctic, *Probl. Arkt. Antarkt.*, *11*, 59–64, 1962.

Yen, Y. C., K. C. Cheng, and S. Fukusako, Review of intrinsic thermophysical properties of snow, ice, sea ice, and frost, in *Proceedings of the 3rd International Symposium on Cold Regions Heat Transfer, Fairbanks, AK, June 11–14, 1991*, edited by J. P. Zarling and S. L. Faussett, pp. 187–218, Univ. of Alaska, Fairbanks, 1991.

H. Eicken, Geophysical Institute, University of Alaska Fairbanks, Fairbanks, AK 99775, USA. (hajo.eicken@gi.alaska.edu)

T. C. Grenfell and B. Light, Department of Atmospheric Sciences, University of Washington, Seattle, WA 98195, USA. (tcg@atmos.washington.edu; bonnie@apl.washington.edu)

D. K. Perovich, J. A. Richter-Menge, and W. B. Tucker III, Engineer Research and Development Center, Cold Regions Research and Engineering Laboratory, 72 Lyme Road, Hanover, NH 03755, USA. (perovich@crrel.usace.army.mil; Jacqueline.A.Richter-Menge@erdc.usace.army.mil; wtucker@crrel.usace.army.mil)